Journal of Inorganic Biochemistry 186 (2018) 116–129

Contents lists available at ScienceDirect

Journal of Inorganic Biochemistry

journal homepage: www.elsevier.com/locate/jinorgbio

Bifunctional 3-hydroxy-4-pyridinones as effective aluminium chelators: synthesis, solution equilibrium studies and *in vivo* evaluation

Anna Irto[a], Paola Cardiano[a], Karam Chand[b], Rosalia Maria Cigala[a], Francesco Crea[a], Concetta De Stefano[a], Lurdes Gano[c], Silvio Sammartano[a,*], Maria Amélia Santos[b,*]

[a] Dipartimento di Scienze Chimiche, Biologiche, Farmaceutiche e Ambientali, Università di Messina, Viale F. Stagno d'Alcontres, 31, 98166 Messina, Italy
[b] Centro de Química Estrutural, Instituto Superior Técnico, Universidade de Lisboa, Av. Rovísco Pais 1, 1049-001 Lisboa, Portugal
[c] Centro de Ciências e Tecnologias Nucleares (C2TN), Instituto Superior Técnico, Universidade de Lisboa, Estrada Nacional 10, 2695-066 Bobadela LRS, Portugal

ARTICLE INFO

Keywords:
3-Hydroxy-4-pyridinones
Speciation
Protonation
Al^{3+} complexation
Sequestering ability
In vivo chelation

ABSTRACT

This paper reports the results on the study of a set of synthesized bifunctional 3-hydroxy-4-pyridinones chelators as potential aluminium sequestering agents. They were *N*-functionalized with alkyl-amino, -carboxylic and –(amino-carboxylic) groups, envisaging the improvement of the Al^{3+} sequestering capacity, in comparison with the marketed chelating drug deferiprone. The main focus of this work was given to the assessment of their binding ability towards Al^{3+}, which was studied by potentiometric and UV–Vis spectrophotometric measurements carried out at $T = 298.15$ K. The speciation models were characterized by $Al_pL_qH_r^{(3p+r-qz)}$ species with different stoichiometry. Depending on ligand side-chain structures and on their thermodynamic properties, different trends of stability was found. Furthermore, the sequestering ability of the ligands towards Al^{3+} was investigated by the calculation of $pL_{0.5}$ values at different experimental conditions. These results clearly indicate that the presence of amino-carboxylic groups in the ligands increases the sequestering ability towards Al^{3+}. The *in silico* evaluation of pharmacokinetic descriptors indicated no violation to the Lipinski's rule and drug-likeness properties. Furthermore, the *in vivo* bioassays on a model of metal-overload mice showed for three investigated ligands a higher metal-sequestering capacity than for the chelating drug deferiprone, thus suggesting their potential interest as Al-chelating drug candidates.

1. Introduction

The treatment of diseases related to the accumulation of hard metal cations in the human body is based on the chelating therapy. This approach consists in the administration of chelators to patients, to induce the sequestration of the metal ions (*e.g.* Fe^{3+}, Al^{3+}, etc.) and their systemic excretion [1–4]. Intake of metals in the human body can occur through the diet, the environment or other external sources; once absorbed, they reach the blood and human organs, competing with other essential metals for vital functions. For a long time the Deferoxamine (DFO or Desferal®), was used as chelator in the treatment of iron overload [5]. It is a microbial trishydroxamic acid [6] able to form with Fe^{3+}, as hexadentate ligand, a metal–ligand complex, having high stability from the thermodynamic point of view ($\log K_{[FeL]^{2+}} = 30.6$ at $I = 0.10$ M in $KCl_{(aq)}$ and $T = 298.15$ K) [7,8]. On the other hand, it is featured by various side effects, such as hydrophilic character, oral inactivity, toxicity, being also very expensive [9]. To overcome these drawbacks, the employment of a new class of chelating agents has been developed, *i.e.* the family of 3-hydroxy-4-pyridinones (3,4-HPs), derivatives of 1,2-dimethyl-3-hydroxy-4-pyridinone, commercially known as deferiprone (DFP) or Ferriprox®, and approved as oral drug for the treatment of patients affected by iron overload. These molecules are a class of bidentate compounds, characterized by an aromatoid *N*-heterocycle with hydroxyl and ketone groups in ortho position. Unlike DFO, 3,4-HPs can be effective in all biological conditions, do not cause undesired effects and are also economically affordable [10–13]. These products can be synthesized from maltol, a natural origin compound [14].

The 3,4-HP herein studied are extra-functionalized (*see* Fig. 1), envisaging the improvement of their affinity towards biological sites and drug-likeness properties. Although some of these compounds (*L1*: 4-(3-hydroxy-2-methyl-4-oxopyridin-1(4H)-yl)butanoic acid; *L5*: 1-(3-aminopropyl)-3-hydroxy-2-methylpyridin-4(1H)-one; *L4*: (*S*)-2-amino-5-(3-hydroxy-2-methyl-4-oxopyridin-1(4H)-yl)pentanoic acid) have already been studied by some of the authors [15–17], the fact that the ligand with the amino-carboxylic side chain (*L4*) presented a good *in vivo*

* Corresponding authors.
E-mail addresses: ssammartano@unime.it (S. Sammartano), masantos@ist.utl.pt (M.A. Santos).

https://doi.org/10.1016/j.jinorgbio.2018.05.017
Received 14 February 2018; Received in revised form 25 May 2018; Accepted 26 May 2018
Available online 30 May 2018
0162-0134/

Abbreviations table

DFB	Deferoxamine or Desferal®
DFP	1,2-dimethyl-3-hydroxy-4-pyridinone, deferiprone or Ferriprox®
L1	4-(3-hydroxy-2-methyl-4-oxopyridin-1(4H)-yl)butanoic acid
L2	(*S*)-2-amino-4-((2-(3-hydroxy-2-methyl-4-oxopyridin-1(4H)-yl)ethyl)amino)-4-oxobutanoic acid
L3	(*S*)-2-amino-4-((3-(3-hydroxy-2-methyl-4-oxopyridin-1(4H)-yl)propyl)amino)-4-oxobutanoic acid;
L4	(*S*)-2-amino-5-(3-hydroxy-2-methyl-4-oxopyridin-1(4H)-yl)pentanoic acid
L5	1-(3-aminopropyl)-3-hydroxy-2-methylpyridin-4(1H)-one
EthylL	2-(3-hydroxy-2-ethyl-4-oxopyridin-1(4H)-yl)acetic acid
UV–Vis spectrophotometry	Ultraviolet-Visible spectrophotometry
NMR	Nuclear Magnetic Resonance
ESI-MS	Electrospray Ionization Mass Spectroscopy
MS-LC Ion Trap	Mass-Liquid Chromatography Ion Trap
BnCl	benzyl chloride
MeOH	methanol
EtOH	ethanol
10% Pd/C	palladium on activated carbon, 10% (w/w)
TLC	Tin Layer Chromatography
DCM	dichloromethane
DMF	*N*-dimethylformamide
DMSO	dimethyl sulfoxide
ACN	acetonitrile
Et_2O	diethyl ether
TMS	tetramethylsilane

performance in terms of metal clearance, led us to develop other two new analogues (*L2:* (*S*)-2-amino-4-((2-(3-hydroxy-2-methyl-4-oxopyridin-1(4H)-yl)ethyl)amino)-4-oxobutanoic acid; *L3:* (*S*)-2-amino-4-((3-(3-hydroxy-2-methyl-4-oxopyridin-1(4H)-yl)propyl)amino)-4-oxobutanoic acid) containing the same terminal group but with an extra amide bond. So the set of five bifunctional ligands containing as side groups amino-carboxylic, as well as amino, carboxylic groups (for comparison purposes) were prepared and evaluated for their Al^{3+}-sequestering capacity. Their preparation involved standard reactions of maltol with bifunctional amines, while in some cases further coupling reactions with a cyclic amino-acid anhydride with the formation of new amidic bonds [5,11–13]. The synthetic procedures used in the preparation of a set of the bifunctional 3-hydroxy-4-pyridinones are schematically described in Scheme 1. The acid-base properties were investigated by Ultraviolet-Visible (UV–Vis) spectrophotometry, spectrofluorimetry, while the binding ability towards Al^{3+} was studied by potentiometry and UV–Vis spectrophotometry. With the purpose of confirming the speciation models proposed on the basis of the cited investigations, the protonation behavior of *L2* as well as its interaction with Al^{3+} was further studied by ^{1}H Nuclear Magnetic Resonance (NMR) spectrometry. The measurements were carried out at $I = 0.15$ M

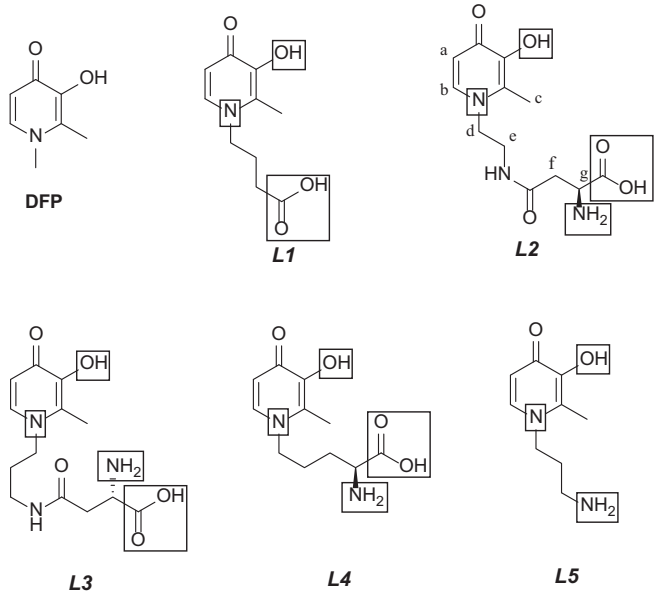

Fig. 1. Structures of deferiprone (DFP) and bifunctional 3-hydroxy-4-pyridinones under study. For *L2*, the letters stand for the ^{1}H NMR titrations peaks assignment. For each ligand the protonable groups are highlighted.

in NaCl, the main inorganic component of most of natural [18,19] and biological fluids [20]. The investigations on the acid-base properties of these 3-hydroxy-4-pyridinones (3,4-HPs) were performed at $T = 298.15$ and 310.15 K, with the aim of assessing their behavior also at physiological conditions. To complete this study, the sequestering ability of the ligands towards the Al^{3+} was investigated, by means of a sigmoidal equation and of $pL_{0.5}$ parameter, previously proposed by the research group [21]. *In vivo* assays on metal-sequestration of a ^{67}Ga treated mice model were also carried out for the 3,4-HP-amino-acid derivatives (*L2, L3, L4*) in comparison with the market drug (DFP).

2. Materials and methods

2.1. Chemicals for solution studies

All the reagents were of the highest available purity and the solutions were prepared with analytical grade water ($R = 18\,M\Omega\,cm^{-1}$) using grade A glassware. Hydrochloric acid and sodium hydroxide solutions were prepared by diluting concentrated ampoules (Riedel-deHäen) and were standardized against sodium carbonate and potassium hydrogen phthalate, respectively. NaOH solutions were preserved from atmospheric CO_2 using soda lime traps. The aluminium solutions were prepared by weighing $AlCl_3$ hexahydrate, without further purification, and standardized with EDTA standard solutions; their purity resulted always ≥98% [22]. NaCl aqueous solutions were prepared by weighing the pure salt (Fluka), previously dried in an oven at $T = 383.15$ K for at least 2 h.

2.2. General synthetic information

Analytical grade reagents were purchased from Sigma-Aldrich, Fluka and Acros and were used as supplied. The solvents, if necessary, were dried according to standard methods [23]. All the reactions were TLC (Tin Layer Chromatography) controlled and the most common used mobile phases were dichloromethane (DCM): methanol (MeOH): ammonium hydroxide (NH_4OH) solvents mixtures: S1 (DCM-MeOH 9.5:0.5), S2 (DCM-MeOH-NH_4OH 8.5:1:0.5), S3 (DCM-MeOH-NH_4OH 8:2:0.5) (for more details *see* Abbreviations table). Moreover, ferric chloride (to check the presence of phenol groups), ninhydrine (for amino groups) and Dragendorff's reagent (if quaternary nitrogen groups were present) assays were carried out. The purity of the synthesized compounds was checked by ^{1}H and ^{13}C NMR (proton and 13-carbon Nuclear Magnetic Resonance) experiments, performed with Bruker AVANCE III 300 MHz and 400 MHz spectrometers, in deuterated solvents (D_2O, Methanol-d_4, Dimethyl sulfoxide-d_6 (DMSO-d_6)). Melting point of each 3-hydroxy-4-pyridinone was measured using a Leica Galen III hot stage apparatus. The following abbreviations are used: s = singlet, d = doublet, t = triplet, m = multiplet. Electrospray

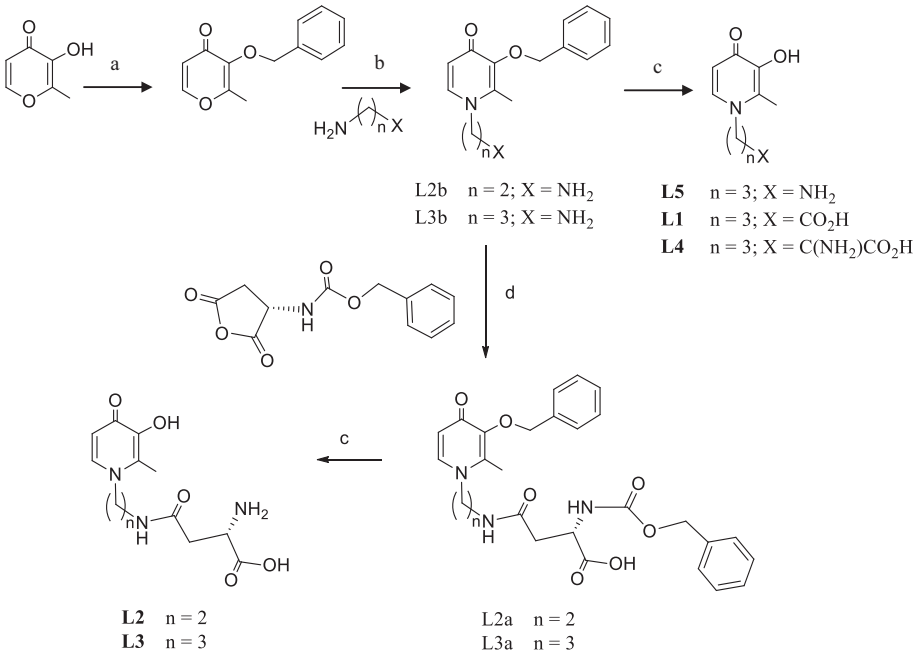

Scheme 1. General scheme for the synthesis of the ligands. Reagents and conditions: a) BnCl, NaOH, MeOH/H_2O, reflux T = 348 K, 20 h; b) NaOH, EtOH/H_2O, reflux T = 348 K, 20 h; c) H_2, 10% Pd/C, MeOH, p = 4.5 atm, 3–4 h; d) dry DMF, T = 333 K, 3 h.

ionization mass (ESI-MS) spectra were carried out on a 500 MS-LC (Mass-Liquid Chromatography) Ion Trap (Varian Inc., Palo Alto, CA, USA) mass spectrometer equipped with an ESI ion source, operated in the positive or negative ion mode. For the target final compounds, the elemental analyses were performed on a Fisons EA1108 CHNS/O instrument at LAIST and were within the limit of ± 0.4%.

2.3. Synthetic procedures

2.3.1. Synthesis of 4-(3-hydroxy-2-methyl-4-oxopyridin-1(4H)-yl)butanoic acid (L1)

This compound was prepared following a synthetic procedure previously described [24].

2.3.2. Synthesis of (S)-2-amino-4-((2-(3-hydroxy-2-methyl-4-oxopyridin-1(4H)-yl)ethyl)amino)-4-oxobutanoic acid (L2)

2.3.2.1. 3-(Benzyloxy)-2-methyl-4-pyrone. To a solution of 3-hydroxy-2-methyl-4H-pyran-4-one (20.07 g, 159.15 mmol) in 200 mL of MeOH, a solution of sodium hydroxide (6.98 g, 174.50 mmol) in 22 mL of water was added to this mixture, followed by dropwise addition of benzyl chloride (22.0 mL, 191.00 mmol). The reaction mixture was heated to reflux at T = 348 K for 12 h. The solvent was evaporated under reduced pressure and the remaining orange oil was dissolved in DCM (80 mL) and washed with 5% (w/v) of NaOH aqueous solution (3 × 30 mL) and with water (2 × 30 mL). The organic phase was dried over anhydrous sodium sulfate and filtered. The solvent was roto-evaporated and dried in vacuum to give a pale yellow oil product (32.93 g, η = 95%). TLCs were performed in S1 mixture. ^{1}H NMR (400 MHz, Methanol-d_4), δ (ppm): 7.82 (1H, d, 6-*H*Py), 7.33 (5H, s, Ph), 6.35 (1H, d, 5-*H*Py), 5.03 (2H, s, CH_2Ph), 2.05 (3H, s, CH_3). ^{13}C NMR (100 MHz, Methanol-d_4), δ(ppm): 175.81, 160.98, 155.05, 143.49, 136.81, 128.76, 128.19, 128.18, 116.22, 73.37, 13.67; *m/z* (ESI-MS) = 217 (M + 1).

2.3.2.2. 1-(2-Aminoethyl)-3-(benzyloxy)-2-methylpyridin-4(1H)-one. 3-Benzyloxy-2-methyl-4-pyrone (20.18 g, 93.35 mmol) was dissolved in a EtOH (ethanol)/H_2O mixture (6/8 mL) and added dropwise to a mixture of ethylenediamine (6.90 mL, 102.66 mmol) in 37 mL of ethanol and 24 mL of water, and 8.5 mL of a NaOH aqueous solution (c_{NaOH} = 2 M). This reaction mixture was left under reflux at T = 348 K for 20 h. After cooling, HCl aqueous solution (c_{HCl} = 2 M) was added until pH ~1 and ethanol was evaporated. To the remaining oily solution, water was added (50 mL), followed by extraction with diethyl ether (4 × 50 mL). The aqueous phase was alkalinized with NaOH aqueous solution (c_{NaOH} = 10 M) until about pH ~ 12 and extracted with dichloromethane (3 × 50 mL). The organic phase was dried over anhydrous sodium sulfate and filtered; then the solvent was evaporated to dryness. To this dried residue, 3 mL of EtOH were added; this solution was acidified until pH ~2 with HCl-saturated EtOH to give a white precipitate that was recrystallized from EtOH-ACN (ACN: acetonitrile), providing a pure product as the corresponding hydrochloride salt (8.80 g, η = 32%). TLCs in S2 mixture, R_f = 0.74. m.p. 460–463 K. ^{1}H NMR (400 MHz, D_2O), δ (ppm): 8.12 (1H, d, 6-*H*Py), 7.39 (5H, s, Ph), 7.10 (1H, d, 5-*H*Py), 5.07 (2H, s, CH_2Ph), 4.51 (2H, t, CH_2NPy), 3.34 (2H, t, CH_2NH$_2$), 2.36 (3H, s, CH_3). ^{13}C NMR (100 MHz, D_2O), δ (ppm): 166.39, 150.03, 143.49, 142.28, 135.21, 129.62, 129.26, 128.84, 114.09, 75.39, 52.37, 38.00, 12.91; *m/z* (ESI-MS) = 259 (M + 1).

2.3.2.3. (S)-4-((2-(3-(Benzyloxy)-2-methyl-4-oxopyridin-1(4H)-yl)ethyl) amino)-2-(((benzyloxy) carbonyl)amino)-4-oxobutanoic acid (L2a). 1-(2-aminoethyl)-3-(benzyloxy)-2-methylpyridin-4(1H)-one (0.76 g, 2.59 mmol), in the form of hydrochloride salt, was neutralized with potassium hydroxide (0.22 g, 3.92 mmol) in 10 mL of dry MeOH and left stirring under nitrogen for 1 h. After filtering this solution, to remove the white precipitate of KCl and evaporating the solvent under vacuum, 10 mL of DMF (*N*-dimethylformamide), dried with molecular sieves and distilled, were added to the flask. Meanwhile, *N-Z-L*-aspartic anhydride (0.78 g, 3.13 mmol, Z = benzyloxycarbonyl protecting group) was dissolved in 5 mL of dried and distilled DMF and added dropwise to the neutralized protected 3-hydroxy-4-pyridinone. The mixture was left on stirring at T = 333 K under nitrogen. After 3 h, the starting materials were completely consumed and only one major product was formed. The solvent was evaporated under vacuum at *ca.* T = 363 K and the solid product (0.57 g, η = 44%) was obtained after recrystallization with MeOH-Et_2O (Et_2O: diethyl ether). S3 mixture was used as eluent for TLC control of the reaction, R_f = 0.30; m.p. 370–372 K. ^{1}H NMR (400 MHz, Methanol-d_4),

δ (ppm): 7.94 (1H, d, 6-*H*Py), 7.46 (5H, s, Ph(Z)), 7.37 (5H, s, Ph), 6.91 (1H, d, 5-*H*Py), 5.13 (2H, s, C*H*$_2$Ph(Z)), 5.11 (2H, s, C*H*$_2$Ph), 4.56 (1H, t, CH$_2$C*H*NH), 4.31 (2H, t, C*H*$_2$NPy), 3.52 (2H, t, C*H*$_2$NHCO), 2.77 (2H, m, C*H*$_2$CHNH), 2.42 (3H, s, C*H*$_3$). ^{13}C NMR (100 MHz, Methanol-*d*$_4$), δ (ppm): 172.47, 172.24, 171.26, 168.48, 156.93, 147.97, 147.31, 144.91, 136.45, 128.71, 128.66, 128.23, 128.10, 127.65, 127.49, 113.88, 74.13, 65.85, 54.09, 51.55, 38.36, 35.96, 12.01; *m/z* (ESI-MS) = 508 (M + 1).

2.3.2.4. (S)-2-Amino-4-((2-(3-hydroxy-2-methyl-4-oxopyridin-1(4H)-yl) ethyl)amino)-4-oxobutanoic acid (L2). To a solution of (*S*)-4-((2-(3-(benzyloxy)-2-methyl-4-oxopyridin-1(4H)-yl)ethyl)amino)-2-(((benzyloxy)carbonyl)amino)-4-oxobutanoic acid (*L2a*) (0.60 g, 1.18 mmol) in of dry methanol (50 mL), 10% Pd/C (palladium on activated carbon, 10% (w/w), 0.13 g, 1.20 mmol) was added and the mixture was shaked under hydrogen (p = 4.5 atm) for 3 h at room temperature. After filtration of the reaction mixture and evaporation of the solvent under reduced pressure, the solid product was recrystallized with MeOH-Et$_2$O, affording pure *L2* product (0.20 g, η = 52%). TLCs were performed using S3 mixture as mobile phase, R_f = 0.38. m.p. 390–393 K. ^{1}H NMR (400 Hz, D$_2$O), δ (ppm): 7.66 (1H, d, 6-*H*Py), 6.69 (1H, d, 5-*H*Py), 4.30 (2H, t, C*H*$_2$NPy), 3.86 (1H, t, CH$_2$C*H*NH$_2$), 3.55 (2H, t, C*H*$_2$NHCO), 2.68 (2H, m, C*H*$_2$CHNH$_2$), 2.47 (3H, s, C*H*$_3$). ^{13}C NMR (100 MHz, D$_2$O), δ (ppm): 174.56, 172.65, 171.47, 169.59, 164.25, 143.25, 139.26, 111.54, 54.36, 51.32, 38.15, 35.05, 11.08; *m/z* (ESI-MS) = 284 (M + 1). Elemental analysis calcd. for C$_{12}$H$_{17}$N$_3$O$_5$·0.18 H$_2$O: C 50.30, H 6.11, N 14.67%; found: C 50.19, H 6.15, N 14.52%.

2.3.3. Synthesis of (S)-2-amino-4-((3-(3-hydroxy-2-methyl-4-oxopyridin-1(4H)-yl)propyl)amino)-4-oxobutanoic acid (L3)

2.3.3.1. 1-(3-Aminopropyl)-3-(benzyloxy)-2-methylpyridin-4(1H)-one. A solution of 3-benzyloxy-2-methyl-4-pyrone (10.41 g, 48.16 mol) in a ethanol/water mixture (6/4 mL) was added dropwise to a solution of 1,3-diaminopropane (4.50 mL, 52.97 mmol) in a 17 mL of EtOH, 13 mL of H$_2$O and NaOH aqueous solution (c_{NaOH} = 2 M, 4.50 mL). The reaction mixture was left on stirring under reflux at T = 348 K for 20 h. The experimental procedure followed for the workup was the same reported for the 1-(2-aminoethyl)-3-(benzyloxy)-2-methylpyridin-4(1H)-one. Recrystallization of the white precipitate from EtOH-ACN gave the product in the form of hydrochloride salt (5.32 g, η = 36%). TLC control of the reaction was carried out using S2 mixture, R_f = 0.45. m.p. 463–466 K. ^{1}H NMR (400 MHz, D$_2$O), δ (ppm): 8.13 (1H, d, 6-*H*Py), 7.38 (5H, s, Ph), 7.11 (1H, d, 5-*H*Py), 5.08 (2H, s, C*H*$_2$Ph), 4.28 (2H, t, C*H*$_2$NPy), 2.99 (2H, t, C*H*$_2$NH$_2$), 2.34 (3H, s, CH$_3$), 2.09 (2H, m, CH$_2$C*H*$_2$NH$_2$). ^{13}C NMR (100 MHz, D$_2$O), δ (ppm): 164.96, 150.10, 142.97, 141.92, 135.19, 129.69, 129.27, 128.82, 113.56, 75.43, 53.21, 36.21, 27.28, 12.90; *m/z* (ESI-MS) = 273 (M + 1).

2.3.3.2. (S)-4-((3-(3-(Benzyloxy)-2-methyl-4-oxopyridin-1(4H)-yl) propyl)amino)-2-(((benzyloxy)carbonyl)amino)-4-oxobutanoic acid (L3a). 1-(3-Aminopropyl)-3-(benzyloxy)-2-methylpyridin-4(1H)-one hydrochloride salt (1.00 g, 3.24 mmol) was firstly neutralized with KOH (0.25 g, 4.45 mmol) in of dry MeOH (20 mL) under N$_2$ and left stirring for 1 h. The solid precipitate was filtered off, the solvent was rotoevaporated and the residue was dry under vacuum. *N-Z-L*-aspartic anhydride (0.98 g, 3.93 mmol) dissolved in 5 mL of dry and freshly distilled DMF was added dropwise to the neutralized 1-(3-aminopropyl)-3-(benzyloxy)-2-methylpyridin-4(1H)-one dissolved in the same solvent (15 mL). The reaction mixture was left on stirring at T = 333 K under nitrogen for 3 h. Then, DMF was evaporated under vacuum at about T = 366 K and the solid residue was dried under vacuum. Recrystallization from methanol-diethyl ether afforded the desired product (0.37 g, η = 22%); m.p. 378–381 K. The eluent used for the TLC control of the reaction was S3 mixture, R_f = 0.45. ^{1}H NMR (400 MHz, Methanol-*d*$_4$), δ (ppm): 8.05 (1H, d, 8 Hz, 6-*H*Py), 7.37 (5H, s, Ph(Z)), 7.33 (5H, s, Ph), 7.27 (1H, d, 5-*H*Py), 5.16 (2H, s, C*H*$_2$Ph(Z)), 5.12 (2H, s, C*H*$_2$Ph), 4.63 (1H, t, CH$_2$C*H*NH), 4.12 (2H, t, C*H*$_2$NPy), 3.21 (2H, d, C*H*$_2$CHNH), 2.81 (2H, t, C*H*$_2$NHCO), 2,34 (3H, s, CH$_3$), 1.97 (2H, m, CH$_2$C*H*$_2$NH$_2$). ^{13}C NMR (100 MHz, Methanol-*d*$_4$), δ (ppm): 172.97, 172.27, 167.93, 157.02, 147.46, 144.37, 140.90, 136.72, 136.19, 128.81, 128.35, 128.21, 128.07, 127.64, 127.38, 113.93, 74.18, 66.6, 53.20, 51.92, 37.60, 35.38, 29.80, 11.85; *m/z* (ESI-MS) = 522 (M + 1).

2.3.3.3. (S)-2-Amino-4-((3-(3-hydroxy-2-methyl-4-oxopyridin-1(4H)-yl) propyl)amino)-4-oxobutanoic acid (L3). To a solution of L3a (0.33 g, 0.63 mmol) in dry methanol (50 mL), 10% Pd/C (0.09 g, 0.79 mmol) was added and the mixture was shaked under H$_2$ (4.5 atm) for 4 h at room temperature. After filtration of the reaction mixture and evaporation of the methanol under reduced pressure, the solid product was recrystallization from MeOH-Et$_2$O, affording pure *L3* compound (0.15 g, η = 70%). TLCs in mobile phase S3 mixture, R_f = 0.35; m.p. 400–403 K. ^{1}H NMR (400 MHz, methanol-d$_4$), δ (ppm): ^{1}H NMR (400 MHz, D$_2$O), δ(ppm): 7.78 (1H, d, 6-HPy), 6.72 (1H, d, 5-HPy), 4.15 (2H, t, CH$_2$NPy), 3.95 (1H, t, CH$_2$CHNH$_2$), 3.23 (2H, t, CH$_2$NHCO), 2.78 (2H, m, CH$_2$CHNH$_2$), 2,45 (3H, s, CH$_3$), 1.97 (2H, m, CH$_2$CH$_2$NH). ^{13}C NMR (100 MHz, D$_2$O), δ (ppm): 175.02, 172.92, 169.38, 165.15, 143.76, 139.79, 138.59, 137.80, 53.00, 48.90, 36.73, 35.09, 29.13, 11.78; *m/z* (ESI-MS) = 298 (M + 1). Elemental analysis calcd. for C$_{13}$H$_{19}$N$_3$O$_5$·0.1EtOH: C 52.12, H 6.48, N 13.92%; found: C 52.23, H 6.51, N 13.86%.

2.3.4. Synthesis of (S)-2-amino-5-(3-hydroxy-2-methyl-4-oxopyridin-1(4H)-yl)pentanoic acid (L4)

Compound *L4* was synthesized using a protocol already reported in the literature [15].

2.3.5. Synthesis of 1-(3-aminopropyl)-3-hydroxy-2-methylpyridin-4(1H)-one (L5)

This product was prepared following literature procedures described previously [17].

2.4. Experimental equipments and procedures

2.4.1. UV–Vis spectrophotometric apparatus and procedure

A Varian Cary 50 UV–Vis spectrophotometer equipped with an optic fiber probe with a fixed 1 cm path length was used for performing the spectrophotometric measurements. The instrument was connected to a PC and the acquisition of the signal, the absorbance (A) *vs.* wavelength (λ/nm) was carried out by the Varian Cary WinUV software. At the same time, potentiometric data were collected using a combined glass electrode (Ross type 8102, from Thermo-Orion), connected to a potentiometric apparatus. The titrant was delivered in the measurement cell by means of a Metrohm 665 automatic burette; a stirring bar ensured the homogeneity of the solutions during the experiment. Before each measurements, $N_{2(g)}$ was bubbled in the solutions for at least 5 min, with the aim of excluding the presence of $CO_{2(g)}$ and $O_{2(g)}$.

For the investigation of the 3-hydroxy-4-pyridinones protonation constants, 25 mL of a solution containing the ligands ($1.2{\cdot}10^{-5} \le c_L$ / M ≤ $5.5{\cdot}10^{-5}$) was titrated in the pH range 2.0–10.7. The measurements were performed in the range 200 ≤ λ/nm ≤ 400 at I = 0.15 M in NaCl$_{(aq)}$ and T = 298.15 K and 310.15 K (physiological conditions). For the study of the aluminium-ligand interactions, the titrations were carried out in the wavelengths range as for the study of the acid-base properties. The following metal and ligand concentrations were used: Al^{3+} ($5{\cdot}10^{-6} \le c_{Al^{3+}}$ / M ≤ $1.5{\cdot}10^{-5}$), ligands ($1.2{\cdot}10^{-5} \le c_L$ / M ≤ $5.5{\cdot}10^{-5}$), at I = 0.15 M in NaCl$_{(aq)}$ and T = 298.15 K, in the pH range 2.0–11.0.

2.4.2. Spectrofluorimetric apparatus and procedure

A FluoroMax-4 spectrofluorometer by Horiba Jobin-Yvon, equipped with F-3006 Autotitration Injector with two Hamilton Syringes (mods.

Gastight 1725 and 1001 TLLX, 250 μL and 1 mL of capacity, respectively), was used for performing the experiments; the resolutions of wavelength selectors and titrant additions were 0.3 nm and 0.25 μL, respectively. The spectrofluorometer was equipped with a Peltier Sample Cooler (mod. F-3004) controlled by a Peltier Thermoelectric Temperature Controller model LFI-3751 (5 A - 40 W). The system was controlled by the FluorEssence 2.1 software by Horiba Jobin-Yvon. The measurements were performed using a 1 cm light path Hellma type 101-OS precision cell. In this cell a magnetic stirrer to homogenize the solution and a combined glass microelectrode (model biotrode 6.0224.100 purchased from Metrohm) to measure the e.m.f. or the pH were inserted. The burette tip and the electrode were both located to avoid interference with the light beam. The automatic acquisition of data, in term of emission intensity *vs.* λ/nm for each volume of titrant added, was performed using the same FluorEssence 2.1 software. The best experimental conditions were determined through preliminary evaluations in which parameters such as equilibration time, scan rate, scan range and integration time, excitation and emission wavelengths, were systematically changed to select the values providing the best signal/noise ratio.

Spectrofluorimetric measurements were performed at $I = 0.15$ M in $NaCl_{(aq)}$ and $T = 298.15$ K and 310.15 K. The experiments were carried out by titrating, with NaOH standard solutions, 2 mL of a solution containing the ligands in the concentration range $5{\cdot}10^{-4} \le c_L / M \le 1{\cdot}10^{-3}$ and NaCl to obtain the desired ionic strength. After each addition of base, the intensity of signal (counts per second, CPS) was recorded in the wavelengths range $300 \le \lambda/nm \le 520$ (excitation wavelength: $\lambda/nm = 278$), with a scan rate of $2\,nm\,s^{-1}$ and an integration time of 0.5 s, together with the corresponding e.m.f. value.

2.4.3. Potentiometric apparatus and procedure

Potentiometric measurements were carried out at $I = 0.15$ M in $NaCl_{(aq)}$ and $T = 298.15$ K by using a Metrohm model 809 Titrando connected to an automatic burette equipped with a combined glass electrode (Ross type 8102, from Thermo-Orion). The apparatus was connected to a PC and automatic titrations were performed by MetrohmTiAMO 1.2 software with the aim of controlling titrant delivery, data acquisition and to check for e.m.f. stability. Estimated accuracy was ± 0.15 mV and ± 0.003 mL for e.m.f. and titrant volume readings, respectively. The titrations were carried out in thermostatted cells under magnetic stirring, bubbling through the solution purified presaturated $N_{2(g)}$ to exclude $O_{2(g)}$ and $CO_{2(g)}$ inside. The measurement solutions were prepared at different Al^{3+} ($5{\cdot}10^{-4} \le c_{Al^{3+}} / M \le 7{\cdot}10^{-4}$) and ligand ($5{\cdot}10^{-4} \le c_L / M \le 2{\cdot}10^{-3}$) concentration to obtain wide metal/ligand molar ratios.

For each experiment, independent titrations of strong acid with standard sodium hydroxide solutions were performed, at the same experimental conditions of ionic medium, ionic strength (I) and temperature (T) of the systems under study, to obtain the value of electrode potential (E^0), the acidic junction potential ($E_j = j_a[H^+]$), and the ionic product of water (K_w). The pH scale used was the free scale, not activity, so $pH = -\log [H^+]$, where $[H^+]$ is the free proton concentration. For each titration, 80–100 data points were collected, and the equilibrium state during titrations was checked, in particular, verifying the necessary time to reach equilibrium and performing back titrations [25].

2.4.4. NMR apparatus and procedure

^1H NMR spectra at $T = 298.15$ K in 9:1 H_2O/D_2O mixture were recorded on a Bruker AMX R-300 operating at 300 MHz by employing presaturation pulse sequence experiments for water signal suppression. The chemical shifts were measured with respect to tetramethylsilane (TMS) and 1,4-dioxane was used as internal reference ($\delta_{dioxane} = 3.70$ ppm). ^1H NMR titrations on Al^{3+}/*L2* systems were performed by adding sodium hydroxide solution to mixtures of the ligand ($8{\cdot}10^{-3} \le c_L / mol\ L^{-1} \le 1{\cdot}10^{-2}$) and various concentrations metal ion ($3.3{\cdot}10^{-3}$–$4{\cdot}10^{-3}$ M), at metal/ligand ratios between 2 and 3, at pH between *approx.* 2.0 and 7.0, and $I = 0.15$ M in $NaCl_{(aq)}$. Prior to the study of metal containing systems, the protonation behavior of *L2* was also investigated for $c_L = 1{\cdot}10^{-2}$ M solutions at $I = 0.15$ M in $NaCl_{(aq)}$, in the pH range 2.0–10.7.

2.5. Calculations

The refinement of all the parameters of the acid–base titration such as E^0, pK_w, liquid junction potential coefficient j_a, analytical concentration of reagents was carried out by means of the non-linear least squares computer program ESAB2M [26]. The determination of the protonation constants from the UV–Vis spectrophotometric and spectrofluorimetric data involved the use of HYPERQUAD 2008 computer program [27]. For *L2* ^1H NMR solution spectra, since all proton exchange reactions were found to be fast on the NMR time-scale, the individual chemical shifts belonging to each species and the relative protonation constants were calculated with the HypNMR computer program [28]. Protonic NMR spectra of Al^{3+}/*L2* solutions showed two sets of resonances, accounting for free and bound ligand, respectively; the bound average chemical shifts were employed in the HypNMR calculations (*see* Results and discussions) thus allowing the refinement of the stability constants as well as the individual NMR parameters of each complex species, keeping constant the "free" *L2* individual chemical shifts previously calculated. The calculation of the formation constants obtained by potentiometric titrations at different ionic strengths and temperatures was carried out by means of BSTAC and HYPERQUAD 2008 computer programs. More details on these latter computer programs used for the elaboration of the experimental data are reported [27,29]. HySS program [27] was used to draw the speciation diagrams and to calculate the species formation percentages.

The protonation constants of all the ligands (L^{z-}) are given according to the stepwise ($\log K_r^H$; Eq. (1) and overall ($\log \beta_r^H$; Eq. (2)) equilibria, respectively:

$$H^+ + H_{(r-1)}L^{-(z-(r-1))} = H_rL^{-(z-r)} \quad (1)$$

and

$$rH^+ + L^{z-} = H_rL^{-(z-r)} \quad (2)$$

where r represents the r-th protonation step and z is the charge of the fully deprotonated ligands.

The overall metal hydrolytic constants ($\log \beta_r^{OH}$) are given as follows:

$$pAl^{3+} + rH_2O = Al_p(OH)_r^{(3p-r)} + rH^+ \quad (3)$$

The overall formation constants ($\log \beta_{pqr}$) for the metal–ligand complexes investigated refer to the following equilibrium:

$$pAl^{3+} + qL^{z-} + rH^+ = Al_pL_qH_r^{(3p+r-qz)} \quad (4)$$

All the protonation and stability constants, concentrations and ionic strengths are expressed in the molar (c, M) concentration scale.

2.6. In vivo metal sequestration studies

^{67}Ga-citrate injection solution was prepared by dilution of ^{67}Ga citrate from Mallinckrodt Medical B.V. with saline to obtain a final radioactive concentration of approximately 7.0–8.0 MBq/100 μL. Biodistribution studies were carried out in groups of 3 female Balb-C mice (randomly bred, Charles River, from CRIFFA, France) weighing *ca.* 22–25 g. Mice were intravenously (i.v.) injected with 100 μL (7.0–8.0 MBq) of ^{67}Ga citrate *via* the tail vein immediately followed by intraperitoneal (i.p.) injection of 0.5 μmol of each ligand in 100 μL saline. Animals were maintained on normal diet *ad libitum* and were sacrificed by cervical dislocation at 1 h and 24 h post-administration. The administered radioactive dose and the radioactivity in sacrificed

animals were measured in a dose calibrator (Capintec CRC25R). The difference between the radioactivity in the injected and sacrificed animal was assumed to be due to whole body excretion. Tissue samples of main organs were then removed for counting in a gamma counter (Berthold LB2111, Berthold Technologies, Germany). Biodistribution results were expressed as percent of injected activity per gram of organ (% I.A./g) and presented as mean values ± Std. Deviation.

3. Results and discussions

3.1. Design and synthesis of the ligands

The 3-hydroxy-4-pyridinone derivatives herein reported (Fig. 1) were designed to have low molecular weight while including extra-functional groups aimed to facilitate the interaction with biological sites and to enable the drug absorption from the gastrointestinal (GI) tract. Thus, besides the hydroxypyridinone chelating cores, the ligands are featured with different type/number of H-bond donor and acceptor groups (*e.g.* −COOH), (−NH_2, −NH_2CH_2COOH, −NHCOR), which are expected to increase their affinity towards biological sites. These functional groups are usually attached to the pyridinone side of the molecules by means of *n*-alkylic spacers, with the aim of improving their lipophilicity, and of consequently enhancing their ability to cross biological membranes. On the other hand, the synthesis of excessively lipophilic ligands should be avoided [15], since they could display high toxicity, due to a too much easy crossing through the membranes or a rapid metabolism for gluconization of the −OH group [30]. *In silico* assessment of the main pharmacokinetic properties, (*see* below, Section 3.8), indicated adequate molecular descriptors for drug-likeness properties and bioavailability.

The route for the synthesis of the 3-hydroxy-4-pyridinone derivatives started from the naturally occurring maltol (3-hydroxy-2-methyl-4H-pyran-4-one), following the reaction general procedure shown in Scheme 1. The first step of the synthetic route involves the –OH group protection by a benzyl group, according to Williamson ethers synthesis starting from alcohols [31,32]. The second step implies a double Michael-type addition of a primary amine (extrafunctionalized with a carboxylic (*L1*), an amine (*L5*) or an amino-carboxylic group (*L4*)) with opening and closure of the heterocyclic ring, according to the procedure by Harris et al. [33,34]. For compounds *L2* and *L3* there was a further extrafunctionalization by reaction of an intermediate containing a *N*-alkylamine side chain with *N*-benzyloxycarbonyl protected aspartic anhydride to provide an amino-carboxylic acid terminal groups. The last step in the synthesis of each compound involved always the removal of the protecting groups (*O*-benzyl for all the compounds and also *N*-benzyloxycarbonyl for *L2* and *L3*) *via* hydrogenolysis catalyzed by 10% Pd/C.

3.2. Acid-base properties of the ligands

All the 3-hydroxy-4-pyridinones synthetized were obtained as $H_r(L)^0$ neutral species; in general, for this kind of compounds, different protonable groups are detected: the −OH on the heterocyclic ring, the amino and carboxylic groups eventually present on the alkylic chain and also the pyridinone nitrogen atom (proton supplied by excess of mineral acid) [16]. The structures of all the investigated compounds are reported in Fig. 1. Analysis of the UV–Vis spectrophotometric data of the ligand featuring the simplest lateral chain, *L1*, allowed the determination of three protonation constants related to the hydroxyl group, the carboxylic group and the pyridinone nitrogen atom. The experimental protonation constants at $I = 0.15$ M in $NaCl_{(aq)}$, at $T = 298.15$ K are reported in Table 1. In Fig. S1, the distribution of the *L1* species is shown. The graph evidences that all the species reach high formation percentages (≥60%), being $[H(L1)]^-$ the main species which is present in all the pH range investigated (2.5–10.7).

L2, L3 and *L4* ligands, unlike *L1*, are featured by an amino group on the alkylic chain, so that four functional groups were considered in the protonation study. In particular, *L2* and *L3* are very similar with the difference of an extra –CH_2 group on *L3* alkylic chain, as already shown in Fig. 1. The protonation constants of *L2* and *L3* determined by UV–Vis spectrophotometric technique at $I = 0.15$ M in $NaCl_{(aq)}$, and $T = 298.15$ K are reported in Table 1. The analysis of the results shows that the acid-base properties of the ligands are influenced by the lateral chain length; in particular, the $\log K^H$ values increase with the length of the alkylic spacer. As a representative example, the profile of the titration curves of the UV–Vis spectrophotometric measurements on *L2* at different pH values is reported in Fig. S2. This figure shows that the absorption spectrum (absorbance (A) *vs.* wavelengths (λ)) varies significantly with pH; this behavior can be explained by considering that the ligand protonated species absorb at different wavelengths. From the analysis of the spectra, it is possible to evidence that, upon pH increasing, the absorption band at 278 nm (λ_{max}) is characterized by an increasing of the intensity up to pH ~ 6.0, then it starts to decrease, undergoing a bathochromic shift. Moreover, some isosbestic points occur at different wavelengths.

The last two 3-hydroxy-4-pyridinones, *L4* and *L5*, differ from each other on a carboxylic group on the end of the lateral chain (*L4*). The data obtained at $I = 0.15$ M in $NaCl_{(aq)}$ and $T = 298.15$ K, by UV–Vis spectrophotometric measurements are reported in Table 1, together with the ones found for the other compounds. The refined constant values of the hydroxyl, amino and pyridinone nitrogen groups for *L4* and *L5* are in good agreement.

To confirm the speciation models obtained by UV–Vis spectrophotometric measurements, spectrofluorimetric titrations were performed as well. Moreover, some checks were also carried out by using

Table 1
Protonation constants[a] of the 3-hydroxy-4-pyridinones obtained by different analytical techniques at $I = 0.15$ M in $NaCl_{(aq)}$ and $T = 298.15$ K.

Analytical technique	$\log\beta_r^H$ ($\log K_r^H$)	*L1*	*L2*	*L3*	*L4*	*L5*
UV–Vis spectrophotometry	$\log\beta_1^H$	9.947 ± 0.007[b]	10.73 ± 0.03	10.93 ± 0.02	11.10 ± 0.09	11.08 ± 0.02
	$\log\beta_2$ ($\log K_2^H$)	14.36 ± 0.09 (4.41)	19.52 ± 0.08 (8.79)	20.70 ± 0.06 (9.77)	20.44 ± 0.07 (9.34)	20.468 ± 0.005 (9.388)
	$\log\beta_3^H$ ($\log K_3^H$)	17.74 ± 0.03 (3.38)	24.17 ± 0.08 (4.65)	25.60 ± 0.01 (4.90)	24.60 ± 0.05 (4.16)	23.68 ± 0.03 (3.21)
	$\log\beta_4^H$ ($\log K_4^H$)	–	27.43 ± 0.08 (3.26)	29.02 ± 0.01 (3.42)	27.87 ± 0.04 (3.27)	–
Spectrofluorimetry	$\log\beta_1^H$	9.90 ± 0.04	10.73 ± 0.03	11.03 ± 0.01	11.00 ± 0.01	11.20 ± 0.03
	$\log\beta_2^H$ ($\log K_2^H$)	14.38 ± 0.04 (4.48)	19.50 ± 0.13 (8.77)	20.38 ± 0.02 (9.35)	19.77 ± 0.03 (8.77)	20.51 ± 0.03 (9.31)
	$\log\beta_3^H$ ($\log K_3^H$)	17.73 ± 0.12 (3.35)	24.18 ± 0.03 (4.68)	25.99 ± 0.04 (5.61)	24.38 ± 0.03 (4.61)	23.70 ± 0.03 (3.17)
	$\log\beta_4^H$ ($\log K_4^H$)	–	27.62 ± 0.04 (3.44)	29.69 ± 0.08 (3.70)	27.75 ± 0.03 (3.37)	–
^{1}H NMR Spectroscopy	$\log\beta_1^H$	–	10.79 ± 0.08	–	–	–
	$\log\beta_2^H$ ($\log K_2^H$)	–	19.37 ± 0.05 (8.58)	–	–	–
	$\log\beta_3^H$ ($\log K_3^H$)	–	24.15 ± 0.07 (4.78)	–	–	–
	$\log\beta_4^H$ ($\log K_4^H$)	–	27.41 ± 0.03 (3.26)	–	–	–

[a] $\log K_r^H$ and $\log\beta r^H$ refer to Eqs. (1)–(2), respectively.
[b] ± Std. deviation.

the isosbestic points as wavelengths of excitation but no variations were observed. At each point of the titration (mL of NaOH strong base), the emission intensity variation *vs.* wavelength was recorded. All the ligands evidenced a lowering of the signal along the pH scale, increasing the basicity of the solution. In Fig. S3 a tridimensional titration curve of the ligand *L2* is reported, as an example, at $I = 0.15$ M in $NaCl_{(aq)}$ and $T = 298.15$ K.

The experimental spectrofluorimetric protonation constants of the 3-hydroxy-4-pyridinones studied at $I = 0.15$ M in $NaCl_{(aq)}$ and $T = 298.15$ K are reported in Table 1.

The temperature effect on the protonation constants of the ligands is dependent on the functional group, being different for the hydroxyl with respect to the one displayed for the other groups (carboxylic, amino and pyridinone nitrogen). Accordingly, analyzing the data reported in Table 2, it appears that generally the $\log\beta_1^H$ values slightly increase with temperature whereas for the other protonation constants this trend is not respected. To better highlight the temperature effect on the speciation, in Fig. 2 the distribution diagram of *L2* at $I = 0.15$ M in $NaCl_{(aq)}$ at $T = 298.15$ K and $T = 310.15$ K is reported. The graph evidences that the formation of the species at $T = 310.15$ K is shifted to lower pH values.

The spectrofluorimetric data, reported in Table 2 at $I = 0.15$ M in $NaCl_{(aq)}$ and $T = 310.15$ K, confirmed the trend of the UV–Vis values, namely a decrease of the protonation constants for the carboxylic, amino groups and pyridinone nitrogen atom upon temperature increasing. Concerning the hydroxyl group, an opposite trend was observed, except for *L1*.

3.3. Hydrolytic constants of Al^{3+}

The acid-base properties of the metal cation (Table S1) were already studied from an accurate analysis of literature data [35–39], at different conditions (*i.e. I*, *T*, etc.) and are reported in a previous paper [40].

3.4. Stability of Al^{3+}/L^{s-} complexes

The study of the interactions of Al^{3+} with the ligands of interest (*L1–L5*), at $I = 0.15$ M in $NaCl_{(aq)}$ and $T = 298.15$ K, allowed to determine $Al_pL_qH_r^{(3p+r-qz)}$ complexes of different stoichiometry. The most reliable speciation models were selected taking into account different variables, namely, (a) the simplicity of the model; (b) the significant formation percentages of the species considered in the pH range investigated; (c) the statistical parameters, as standard deviation on stability constants and on the fit of the systems and in particular (d) the values of corresponding ratios between single variances in comparison with those from the accepted model. The high number of measurements made (and of experimental points collected) allowed us to consider the differences in variance between the accepted model and other models to be significant.

Table 3 reports the experimental overall stability constants of all the

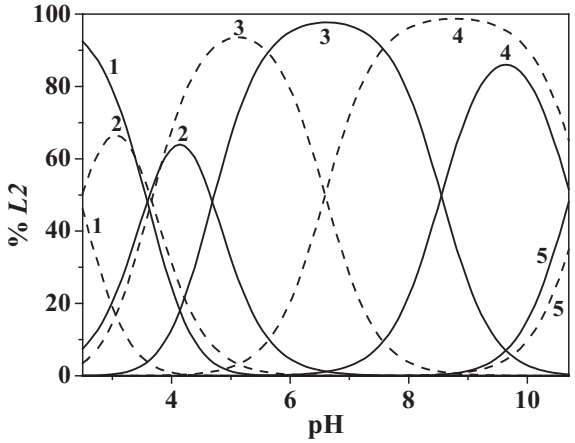

Fig. 2. Distribution diagram of *L2* ($c_L = 3{\cdot}10^{-5}$ M) at $I = 0.15$ M in $NaCl_{(aq)}$ and $T = 298.15$ K (solid line) and $T = 310.15$ K (dashed line). Species: 1. $[H_4(L2)]^{2+}$; 2. $[H_3(L2)]^{+}$; 3. $[H_2(L2)]^{0}$; 4. $[H(L2)]^{-}$; 5. $[(L2)]^{2-}$.

Al^{3+}/3-hydroxy-4-pyridinones complexes obtained by potentiometry (1st column), UV–Vis spectrophotometry (2nd column), ^{1}H NMR spectroscopy (3rd column, *see* ^{1}H NMR titrations section) and an average (4rd column) of the cited values. The pH ranges of the experimental measurements were 2.0–9.2 and 2.0–11.0 from potentiometric and UV–Vis spectrophotometric data, respectively.

The investigation on $Al^{3+}/L1$ interactions allowed to define a speciation model featured by five species, namely $[Al(L1)]^{+}$, $[Al(L1)_2]^{-}$, $[Al(L1)_2H]^{0}_{(aq)}$, $[Al(L1)_2H_2]^{+}$ and $[Al(L1)_3]^{3-}$, without the formation of possible hydrolytic or sparingly soluble species of Al^{3+}.

For the study of the $Al^{3+}/L2$, $Al^{3+}/L3$, $Al^{3+}/L4$ and $Al^{3+}/L5$ systems, where all the ligands contain an amino group, the same speciation model was obtained; this model consists of two species, namely $[AlLH]^{(4-z)}$ and $[AlL]^{(3-z)}$; the UV–Vis spectrophotometric data confirmed the speciation schemes obtained by potentiometry, the stability constant values being also reported in Table 3, found from the two instrumental techniques in good agreement.

Concerning the $[Al(L2)]^{+}$ and $[Al(L3)]^{+}$ species, the stability constant values decrease with alkyl chain length increasing. As an example, Fig. S5 illustrates a comparison between the $Al^{3+}/L2$ system titration curves from potentiometric data at different metal-to-ligand molar ratio. During the experiments the formation of the $[Al(OH)_3]^{0}_{(s)}$ species did not occur; however, introducing the solubility product of the sparingly soluble species in the speciation model of the $Al^{3+}/L3$ system, by means of the HySS computer program, its formation can be expected starting from pH ~6.5. This aspect can be explained in terms of slow formation kinetic of this species [41].

The presence of the carboxylic group in *L4* seems to increase the stability of the species with the metal cation suppressing its hydrolytic tendency and the possible formation of sparingly soluble species. In

Table 2
Protonation constants[a] of the 3-hydroxy-4-pyridinones obtained by UV–Vis spectrophotometry and spectrofluorimetry at $I = 0.15$ M in $NaCl_{(aq)}$ and $T = 310.15$ K.

Analytical technique	$\log\beta_r^H$ ($\log K_r^H$)	*L1*	*L2*	*L3*	*L4*	*L5*
UV–Vis spectrophotometry	$\log\beta_1^H$	10.029 ± 0.007[b]	10.99 ± 0.02	10.93 ± 0.02	11.13 ± 0.03	10.57 ± 0.07
	$\log\beta_2$ ($\log K_2^H$)	13.62 ± 0.01 (3.59)	17.05 ± 0.03 (6.06)	17.71 ± 0.07 (6.78)	17.93 ± 0.04 (6.80)	16.53 ± 0.08 (5.96)
	$\log\beta_3^H$ ($\log K_3^H$)	16.54 ± 0.04 (2.92)	21.02 ± 0.04 (3.97)	22.50 ± 0.05 (4.79)	22.00 ± 0.03 (4.07)	19.53 ± 0.05 (3.00)
	$\log\beta_4^H$ ($\log K_4^H$)	–	24.08 ± 0.05 (3.06)	25.93 ± 0.05 (3.43)	25.30 ± 0.05 (3.30)	–
Spectrofluorimetry	$\log\beta_1^H$	10.05 ± 0.02	10.397 ± 0.002	10.47 ± 0.01	10.05 ± 0.02	10.62 ± 0.20
	$\log\beta_2^H$ ($\log K_2^H$)	13.88 ± 0.01 (3.83)	17.34 ± 0.03 (6.94)	17.96 ± 0.06 (7.49)	17.02 ± 0.05 (7.00)	16.93 ± 0.04 (6.31)
	$\log\beta_3^H$ ($\log K_3^H$)	16.44 ± 0.01 (2.56)	20.69 ± 0.04 (3.35)	22.00 ± 0.07 (4.04)	21.17 ± 0.04 (4.15)	19.74 ± 0.08 (2.81)
	$\log\beta_4^H$ ($\log K_4^H$)	–	22.94 ± 0.07 (2.25)	25.15 ± 0.09 (3.12)	24.27 ± 0.01 (3.10)	–

[a] $\log K_r^H$ and $\log\beta r^H$ refer to Eqs. (1)–(2), respectively.
[b] ± Std. deviation.

Table 3
Experimental overall[a] and average[b] stability constants of Al^{3+}/3-hydroxy-4-pyridinone complexes by potentiometric, UV–Vis spectrophotometric and ^1H NMR spectroscopic data at $I = 0.15$ M in $NaCl_{(aq)}$ and $T = 298.15$ K.

Species	Potentiometry (ISE – H^+)	UV–Vis Spectrophotometry	^1H NMR Spectroscopy	Average stability constants
$[Al(L1)]^+$	12.30 ± 0.04[c]	12.85 ± 0.01[c]	–	12.57 ± 0.23[d]
$[Al(L1)_2]^-$	23.44 ± 0.07	22.90 ± 0.03	–	23.17 ± 0.23
$[Al(L1)_2H]^0_{(aq)}$	27.03 ± 0.12	28.37 ± 0.07	–	27.70 ± 0.36
$[Al(L1)_2H_2]^+$	30.92 ± 0.03	30.20 ± 0.05	–	30.56 ± 0.26
$[Al(L1)_3]^{3-}$	31.66 ± 0.18	31.80 ± 0.07	–	31.73 ± 0.11
$[Al(L2)H]^{2+}$	23.28 ± 0.02	23.66 ± 0.01	23.67 ± 0.15[c]	23.59 ± 0.14
$[Al(L2)]^+$	17.94 ± 0.10	17.94 ± 0.04	17.75 ± 0.16	17.90 ± 0.10
$[Al(L3)H]^{2+}$	24.27 ± 0.03	24.50 ± 0.01	–	24.38 ± 0.15
$[Al(L3)]^+$	17.50 ± 0.10	17.65 ± 0.10	–	17.57 ± 0.12
$[Al(L4)H]^{2+}$	23.48 ± 0.03	23.47 ± 0.01	–	23.47 ± 0.03
$[Al(L4)]^+$	18.32 ± 0.03	18.88 ± 0.02	–	18.60 ± 0.23
$[Al(L5)H]^{3+}$	20.98 ± 0.02	20.05 ± 0.10	–	20.51 ± 0.30
$[Al(L5)]^{2+}$	15.08 ± 0.09	15.08 ± 0.09	–	15.08 ± 0.36

[a] $\log\beta_{pqr}$ refers to Eq. (4).
[b] Values obtained by average of potentiometric, UV–Vis spectrophotometric and ^1H NMR spectroscopic data.
[c] ± Std. Deviation.
[d] errors on weighed data.

Fig. 3a the distribution of the Al^{3+}/*L4* complexes obtained from potentiometric data is shown. The $[Al(L4)H]^{2+}$ species is present in solution along the whole pH range of titration, while the $[Al(L4)]^+$ complex starts to form at pH ~2.7. Fig. 3b shows the distribution of the Al^{3+}/*L5* system at the cited experimental conditions. In the case of *L5*, the absence of the –COOH group, with respect to *L4*, should allow the precipitation of $[Al(OH)_3]^0_{(s)}$, as shown in the "*shaded zone*" represented in the figure, where the formation percentages of Al^{3+}, $[Al(L5)H]^{3+}$ and $[Al(L5)]^{2+}$ species are reported (95%, 96% and 8% at pH ~2.0, ~4.1 and ~4.9, respectively). Once again, for the Al^{3+}/*L5* system the formation of $[Al(OH)_3]^0_{(s)}$ was not observed experimentally, but it was calculated by the HySS program [42], taking into account the pK_{s0} value of the sparingly soluble species in the speciation model.

A trend of stability of the species can be provided on the basis of the investigation carried out on the Al^{3+}/3-hydroxy-4-pyridinone systems, *i.e.* by considering the stability constants of the common $[AlL]^{(3-z)}$ species:

L4 > L2 > L3 > L5 > L1

3.5. ^1H NMR titrations

With the aim to gain more information about acid-base behavior of *L2* as well as its coordination capability towards Al^{3+}, several ^1H NMR spectra on a H_2O/D_2O mixture were collected, both on metal free and metal containing systems, at different concentrations and metal/ligand ratios. Since all the spectra coming from the NMR titrations of *L2* with NaOH showed a single set of average resonances, although several species involved in protonation equilibria are present in solution, fast mutual exchange on the NMR time scale was assumed. In addition, the average chemical shifts of *L2* were pH-dependent, thus all the signals, as a common feature, displayed a shielding effect upon pH increasing. More in detail, both the two doublets detected in the aromatoid region, namely *a* and *b* (Fig. 1) exhibited a significant decrease in their chemical shift in the acidic pH range, indicating that the first deprotonation, as expected, involved the pyridinone nitrogen; then the cited peaks did not change to a great extent up to pH ~ 9.0. From this pH value on, the signals started to shift again, being this effect more pronounced for the resonance indicated as "*a*", suggesting a deprotonation occurring at higher pH, involving a nearby functional group, *i.e.* the hydroxyl group. A trend quite similar to the ones described was detected at pH < 4.0 also for the methylene *d* protons, whereas the signals due to *f* protons were virtually unchanged up to pH ~7.0, starting to shift to lower fields at higher pH. More significantly, the triplet due to *g* −CH− group, which is adjacent to both −COOH and $-NH_2$ groups, underwent significant shielding effect for pH < 4.5 and even stronger at pH > 8.0, according to the deprotonation sequence proposed for similar systems [16,43]. Moreover, since in the pH around neutrality, *L2* ligand should have been twice deprotonated, the spectra recorded at pH ~6.5 can be considered with good approximation as the $[H_2(L2)]^0$ single species spectra (Fig. S4). As already stated, all the spectra from *L2* solutions showed a single set of resonances, arising from the rapidly exchanging species on the NMR time scale. In this sense, each observed chemical shift value corresponds to the mol-fraction weighted average

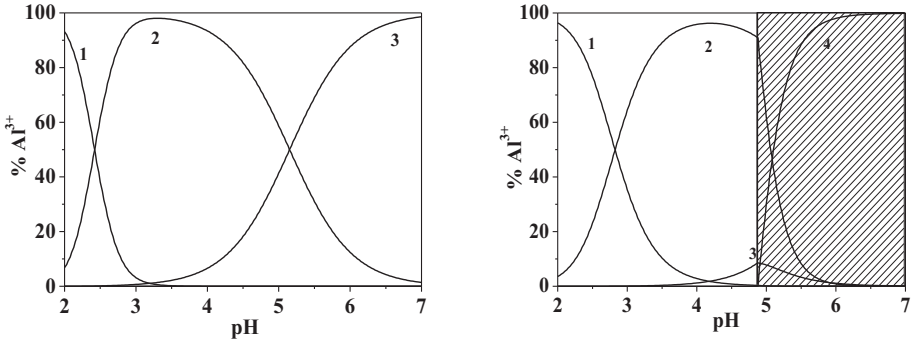

a) (Al^{3+}/*L4*) b) (Al^{3+}/*L5*)

Fig. 3. Distribution diagram of Al^{3+}/*L4* and *L5* systems at $I = 0.15$ M in $NaCl_{(aq)}$ and $T = 298.15$ K, $c_{Al^{3+}} = 8{\cdot}10^{-4}$ M; $c_L = 2{\cdot}10^{-3}$ M: a) *L = L4*, species: 1. free Al^{3+}; 2. $[Al(L4)H]^{2+}$; 3. $[Al(L4)]^+$; b) *L = L5*, species: 1. free Al^{3+}; 2. $[Al(L5)H]^{3+}$; 3. $[Al(L5)]^{2+}$; 4. $[Al(OH)_3]^0_{(s)}$. The pH range from 4.8 to 7.0 ("*shaded zone*") refers to the initial pH value of formation of the sparingly soluble $[Al(OH)_3]^0_{(s)}$ species up to the experimental pH value investigated.

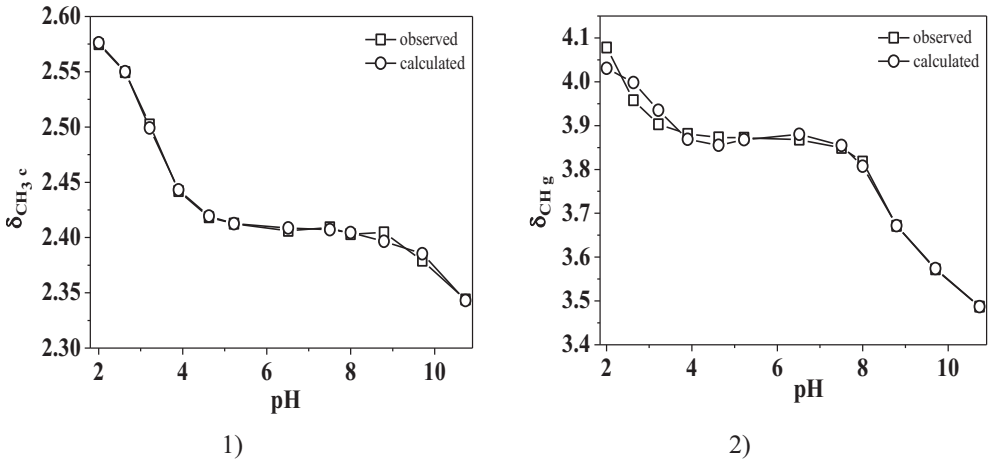

Fig. 4. Observed (□) and calculated (○) values of chemical shifts of *c* (1) and *g* (2) nuclei of *L2 vs.* pH, at $c_L = 1{\cdot}10^{-2}$ M, $I = 0.15$ M in $NaCl_{(aq)}$ and $T = 298.15$ K.

of the values for all the species present at equilibrium, at each investigated pH. The protonation constants and the individual chemical shift values, due to each single species, were obtained by employing HypNMR software. Table 1 shows the calculated protonation constants for *L2,* which are totally consistent with the ones obtained from UV–Vis spectrophotometry and spectrofluorimetry. As can be inferred from Table S2, besides all the peaks due to the differently protonated *L2* species nuclei, the two different resonances due to *f* AB system were refined as well. In addition, experimental and calculated chemical shifts for selected nuclei are compared in Fig. 4, where their excellent agreement is clearly evidenced.

With the purpose of confirming the speciation model proposed for the rationalization of the *L2* complexing capability towards Al^{3+}, ^1H NMR titrations were also carried out for the Al^{3+}/*L2* system, in various concentrations and metal/ligand ratios, as already pointed out in the Materials and methods section. For the spectra collected in the pH range 2.0–5.5, regardless of the metal/ligand ratio employed, two different sets of resonances were observed. More in detail, at lower pH, from the speciation data, together with the $[H_4(L2)]^{2+}$, the formation of $[Al(L2)H]^{2+}$ should be expected. As already observed for several other aluminium-containing systems [44,45], the presence of the metal exerted a general broadening of the spectra; nevertheless, by comparing the spectra recorded at pH ~2.0 for metal free and metal containing systems, the peaks due to $[H_4(L2)]^{2+}$ are clearly distinguishable from the new shielded signals, indicated as "bound" along the discussion (Fig. 5). These new peaks, detected only for *a* and *b* aromatic protons, *c* methyl and *d* methylene, suggest that in the $[Al(L2)H]^{2+}$ metal-ligand interactions, this part of *L2* is involved. It is worth to mention that, differently from the peaks due to the free ligand, the "bound" signals, as long as they could be detectable from the spectra, did not shift to a great extent upon pH increasing. Starting from pH ~5.5, the registered spectra showed a single set of broad bands, although in these conditions signals due to $[Al(L2)]^{+}$ should be observed. In this pH range, the signals named as *a*, *b*, *c*, *d* and *e* appeared downfield shifted with respect to the metal-free system, whereas *f* and *g* peaks were found to be little affected by the presence of aluminium. This experimental evidence suggests that all the species forming from pH ~5.5 on are involved in a fast mutual exchange. Accordingly, the rationalization of the whole NMR data on metal containing systems has been carried out with HypNMR software as well. In this sense, the calculation of the complexes stability constants was carried out using, as known values, the data gained from the protonation data refinement (*i.e.* protonation constants and individual species chemical shifts) obtained previously. The so calculated log*β* values (Table 3) were in excellent agreement with the values derived from potentiometric and spectrophotometric investigations, thus confirming the reliability of the speciation model, as also indicated by the almost total overlapping found for the observed and the calculated average chemical shifts (Fig. S6) found for selected nuclei of the complexes. Furthermore, although from comparison of the experimental spectra collected with and without aluminium, the complexation of *L2* towards Al^{3+} is expected to be accomplished on the pyridinone side of the ligand (*i.e. via* hydroxo-oxo functionality), from the calculated individual chemical shifts of the complexes with respect to the ones refined for the protonated species of *L2* (Table S2), an interaction of metal with $-NH_2$ and/or $-COOH$ could not be discarded.

3.6. Sequestering ability

The simple analysis of the stability constants of metal-ligand complexes is not always sufficient to evaluate the sequestering ability of a ligand towards a metal cation, owing to secondary interactions of the metal or ligand with other components in the system; similar difficulties are observed when the sequestering ability must be estimated at different pH, ionic strengths and temperatures. To solve this issue, it was proposed the introduction of $pL_{0.5}$, an empirical parameter which represents the total concentration of ligand required to sequester the 50% of a metal cation present in trace (10^{-12} M) in solution [21,46].

This parameter is described through a sigmoidal type Boltzmann equation, reported in Eq. (5):

$$x_M = \frac{1}{1 + 10^{(pL - pL_{0.5})}} \quad (5)$$

where x_M is the mole fraction of metal complexed by the ligand, $pL = -\log c_L$ and $pL_{0.5} = -\log c_L$, when $x_M = 0.5$. The sequestering ability can be graphically represented by a dose – response curve, characterized by asymptotes equal to 1 for $pL \rightarrow -\infty$ and 0 for $pL \rightarrow +\infty$, obtained by plotting the mole fraction of the metal complexed *vs.* the pL values. High $pL_{0.5}$ values account for a greater sequestering ability of a ligand towards a metal cation. It is a quantitative and objective parameter which allows to determine the sequestering ability of a ligand in different experimental conditions (pH, ionic strength, ionic medium, temperature), and it is independent on the ion analytical concentration when it is present in trace amount.

Moreover, various factors may influence the systems, such as the protonation of the ligand, the hydrolysis of the metal cation and the interactions with other components, which are taken into account in the speciation model, but are excluded from the calculation of $pL_{0.5}$ values. The estimation of the sequestering ability can be employed for several applications such as remediation of polluted sites, detoxification processes, in chelating therapy and water treatment. All these processes involve the use of a chelating agent, and the assessment of this parameter can be useful for optimizing the working conditions.

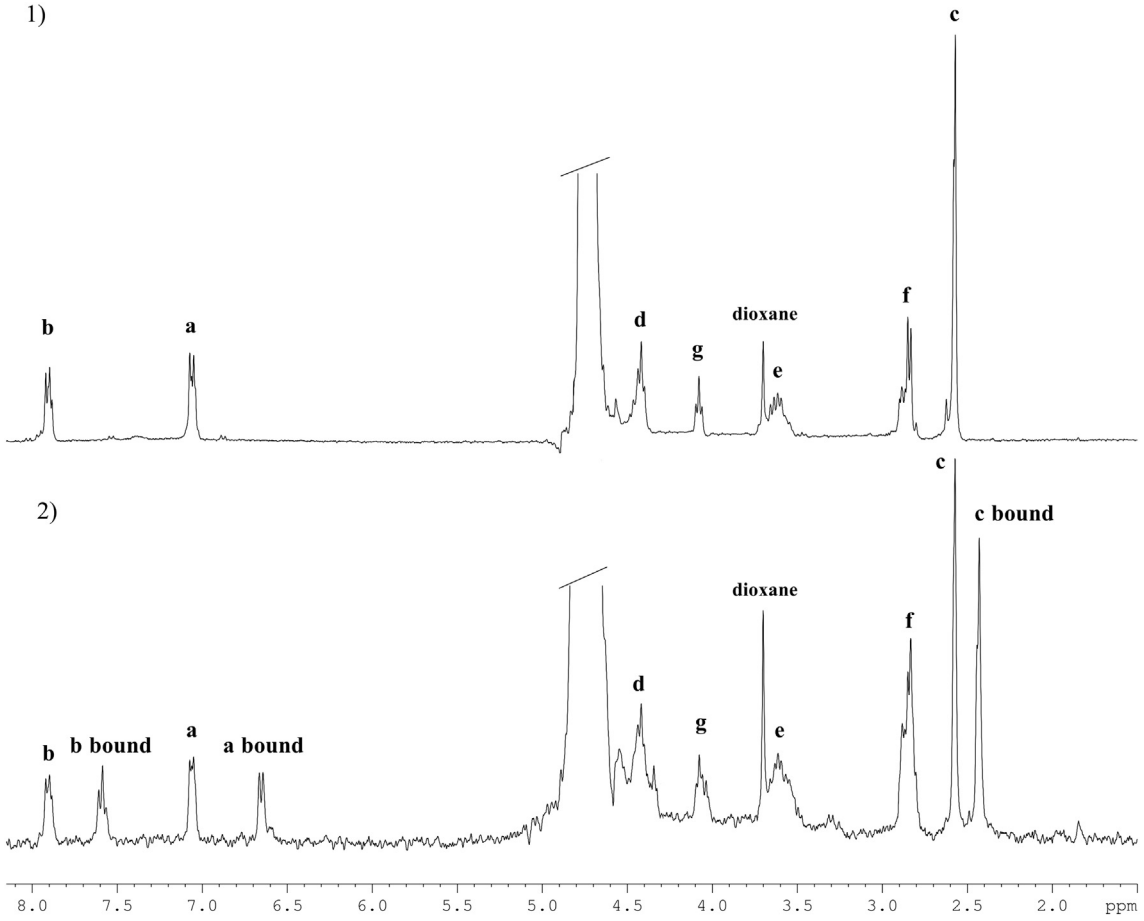

Fig. 5. ^{1}H NMR spectra of: 1) *L2* ($c_L = 1{\cdot}10^{-2}$ M) and 2) Al^{3+}*/L2* system ($c_{Al^{3+}} = 4{\cdot}10^{-3}$ M, $c_L = 8{\cdot}10^{-3}$ M) at pH ~2.0, $I = 0.15$ M in $NaCl_{(aq)}$ and $T = 298.15$ K.

The study of the sequestering ability of the 3,4-HPs towards Al^{3+} was performed at different pH values at $I = 0.15$ M in $NaCl_{(aq)}$ and $T = 298.15$ K. For the Al^{3+}/3-hydroxy-4-pyridinones complexes, the $pL_{0.5}$ values increase with pH, as reported in Table 4. For the Al^{3+}*/L3* and Al^{3+}*/L5* systems at pH > 6.0 the $pL_{0.5}$ values decrease, owing to the possible precipitation of $[Al(OH)_3]^0_{(s)}$. In Fig. 6, an example of sequestration diagram of the *L5* ligand towards Al^{3+} at different pH values is reported. The variations of $pL_{0.5}$ as a function of different parameters such as pH, temperature and ionic strength often follow linear or polynomial patterns, as shown in Fig. S7 for the dependence of $pL_{0.5}$ for the above system on pH.

Table 4
$pL_{0.5}$ values of Al^{3+}/3-hydroxy-4-pyridinones systems from potentiometric data at different pH, $I = 0.15$ M in $NaCl_{(aq)}$ and $T = 298.15$ K.

System	pH	$pL_{0.5}$
Al^{3+}*/L1*	4.0	5.8
Al^{3+}*/L1*	7.0	6.3
Al^{3+}*/L2*	4.0	7.0
Al^{3+}*/L2*	7.0	7.7
Al^{3+}*/L3*	2.0	2.7
Al^{3+}*/L3*	3.5	5.4
Al^{3+}*/L3*	4.0	6.5
Al^{3+}*/L3*	5.0	8.1
Al^{3+}*/L3*	6.0	8.3
Al^{3+}*/L3*	7.0	6.4
Al^{3+}*/L4*	2.5	3.0
Al^{3+}*/L4*	3.5	5.6
Al^{3+}*/L4*	4.0	6.6
Al^{3+}*/L4*	5.0	8.0
Al^{3+}*/L4*	6.0	8.7
Al^{3+}*/L4*	7.0	7.4
Al^{3+}*/L5*	2.5	2.2
Al^{3+}*/L5*	3.0	3.8
Al^{3+}*/L5*	4.0	4.4
Al^{3+}*/L5*	5.0	5.4
Al^{3+}*/L5*	6.0	5.6
Al^{3+}*/L5*	7.0	3.9

From the evaluation of $\log\beta_{110}$ values reported in the Table 3, it would seem that *L4* is featured by the highest capacity to bind the metal cation with respect to the other ligands, while *L1* by the lowest one. On the other hand, the analysis of the $pL_{0.5}$ values calculated from potentiometric data at pH = 4.0 (Table 4), suggested that *L2*, which displays two $-CH_2$ groups on the alkyl chain, unlike all the other compounds bearing propyl groups, shows a higher sequestering ability, that decreases with alkyl chain length increase. Therefore, as already pointed out, the length of the alkylic spacer plays a key role in the coordination behavior of these ligands.

Furthermore, the higher stability constants and $pL_{0.5}$ values determined for the −COOH containing ligands can be an indication that the interaction with Al^{3+} occurs *via* chelation. As it can be observed in Fig. S8 and from the data in Table 4, the $pL_{0.5}$ values for the Al^{3+}*/L5* system are lower than the other ones. This evidence can be confidently attributed to the absence of carboxylate groups in *L5*. Taking into account these considerations and using the stability constants obtained from potentiometric data, at the experimental conditions already mentioned, it is possible to observe the following sequestering ability:

L2 > L4 > L3 > L1 > L5

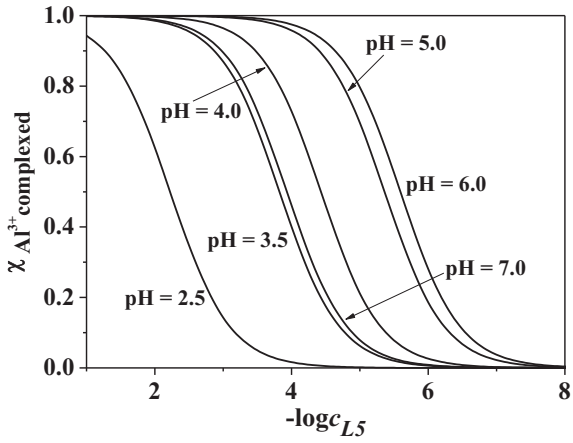

Fig. 6. Sequestration diagram of *L5* ligand towards Al^{3+} at different pH values. Molar fraction of metal cation complexed *vs.* the total ligand concentration (as $-\log c$) at $I = 0.15$ M in $NaCl_{(aq)}$ and $T = 298.15$ K.

3.7. Literature data comparison

The protonaton constants of the 3-hydroxy-4-pyridinones (*L1–L5*) determined in the present paper at $I = 0.15$ M in $NaCl_{(aq)}$ and $T = 298.15$ K, are in good agreement with the ones obtained for deferiprone by Bretti and coworkers [47], Celvette et al. [48] and Ma et al. [49], at the same experimental conditions, as reported in Table 5. Crisponi's group [50–52] and Clarke et al. [53] published the results of DFP protonation studies at $I = 0.10$ M in $KCl_{(aq)}$ and $T = 298.15$ K. Furthermore, Crisponi and coworkers [51] also reported a thermodynamic study on deferiprone acid-base properties at $T = 310.15$ K and different ionic strength values ($I = 0.1$, 0.2, 0.4, 0.5, 1.0 M in $KCl_{(aq)}$).

Santos et al. [16] investigated at $I = 0.10$ M in $KNO_{3(aq)}$ and $T = 298.15$ K the acid-base behavior of *L1* and other 3-hydroxy-4-pyridinones bearing alkylic chains with different length, in particular the 2-(3-hydroxy-2-ethyl-4-oxopyridin-1(4H)-yl)acetic acid, for simplicity here called *EthylL* (2-(3-hydroxy-2-ethyl-4-oxopyridin-1(4H)-yl)acetic acid), a ligand which is featured by an ethylic spacer between the pyridinone nitrogen and the carboxylic group. The protonation constant values of this last compound, reported in Table 5, are lower than the *L1* (propylic spacer) ones here determined at the same temperature and at $I = 0.15$ M in $NaCl_{(aq)}$.

Concerning *L1,* in the same paper Santos et al. [16] characterized the protonable groups, reporting a $\log K_1^H$ attributed to the hydroxyl group, a $\log K_2^H$ to the carboxylic group and a $\log K_3^H$ for the pyridyl nitrogen atom, and values (Table 5) which are in good agreement with those reported in this paper.

The behavior in aqueous solution of *L2* and *L3* could be compared also with that of aspartic acid [37], from which they are derived. The protonation constants for the amino and the carboxylic groups at $I = 0.10$ M in sodium supporting electrolyte and $T = 298.15$ K, stated in Table 5, are in accordance with the corresponding $\log K_2^H$ and $\log K_3^H$ values determined here for *L2* and *L3*.

The acid-base properties of the ligands *L4* and *L5*, were studied by Santos et coworkers [15,17], at $T = 298.15$ K and $I = 0.10$ M in $KNO_{3(aq)}$ and $KCl_{(aq)}$, respectively; they reported values (*see* Table 5) that are fairly in agreement with those here listed, at the already mentioned experimental conditions.

As regards the study of the interactions of the 3-hydroxy-4-pyridinones with Al^{3+}, the stability of $[AlL]^{(3-z)}$ species determined for all the systems at $I = 0.15$ M in $NaCl_{(aq)}$ and $T = 298.15$ K, is higher than the ones found for Al^{3+}/deferiprone system, as published by Clevette et al. [48] and Clarke et al. [53] at the same experimental conditions and at $I = 0.10$ M in $KCl_{(aq)}$ and $T = 298.15$ K. These data are reported in Table 6 for $[AlL]^{(3-z)}$ species. The same trend was observed also by comparing the stability constants obtained for the Al^{3+}/3,4-HPs systems with the Al^{3+}/aspartic acid literature data (Table 6) reported by Martel et al. [37] at the same conditions of temperature and ionic strength employed by Clarke et al. [53], but in Na^+ ionic medium.

Furthermore, the speciation model and the formation constants of Al^{3+}/*L1* complexes obtained in this work are in agreement with the ones determined for the same system by Santos et al. [16] at $I = 0.10$ M in $KNO_{3(aq)}$ and $T = 298.15$ K, as listed in Table 6 for $[AlL]^{(3-z)}$ species. The author also published stability constant values on the Al^{3+}/*EthylL* (two $-CH_2$ groups on the alkylic chain) interactions, which are lower than the corresponding $[Al(L1)]^+$ one, as already seen for the protonation constants, and therefore showing a stability constants increase upon alkylic chain length increasing.

Table 6
Literature stability constants reported for $[AlL]^{(3-z)}$ species at $T = 298.15$ K, different ionic strengths and ionic media.

System	$\log\beta_{110}$	Experimental conditions	Ref.
Al^{3+}/deferiprone	11.91	$I = 0.15$ M in $NaCl_{(aq)}$	[48]
	12.20	$I = 0.10$ M in $KCl_{(aq)}$	[53]
Al^{3+}/aspartic acid	7.87	$I = 0.10$ M in Na^+ supporting electrolyte	[37]
Al^{3+}/*L1*	13.03	$I = 0.10$ M in $KNO_{3(aq)}$	[16]
Al^{3+}/*EthylL*	13.04	$I = 0.10$ M in $KNO_{3(aq)}$	[16]

3.8. In vivo studies on metal sequestering capacity

The efficacy of the new hydroxypyridinone ligands *L2*, *L3* and *L4* as *in vivo* chelating agent for the treatment of aluminium overload was evaluated on the basis of an animal model overload with ^{67}Ga, namely Balb-C mice previously injected with ^{67}Ga-citrate. This option was based on the fact that, as previously reported [13], it has been widely accepted that Ga^{3+}, as an analogue of Fe^{3+} and Al^{3+}, binds to serum proteins, mostly through transferrin and accesses to cells through the transferrin receptor, although there is also evidence that *in vivo* uptake may not be mediated only by this serum protein. For that purpose the

Table 5
Protonation constant values reported in the literature at different ionic strengths, ionic media and at $T = 298.15$ K.

Ligand	$\log K_1^H$	$\log K_2^H$	$\log K_3^H$	$\log K_4^H$	Experimental conditions	Ref.
Deferiprone	9.82	3.69	–	–	$I = 0.15$ M in $NaCl_{(aq)}$	[47]
	9.86	3.70	–	–	$I = 0.15$ M in $NaCl_{(aq)}$	[48]
	9.86	3.84	–	–	$I = 0.15$ M in $NaCl_{(aq)}$	[49]
	9.82	3.66	–	–	$I = 0.10$ M in $KCl_{(aq)}$	[50–52]
	9.77	3.68	–	–	$I = 0.10$ M in $KCl_{(aq)}$	[53]
	9.70	3.57	–	–	$I = 0.10$ M in $KCl_{(aq)}$, $T = 310.15$ K	[50–52]
L1	9.83	4.13	3.34	–	$I = 0.10$ M in $KNO_{3(aq)}$	[16]
EthylL	9.91	4.38	3.53	–	$I = 0.10$ M in $KNO_{3(aq)}$	[16]
aspartic acid	9.66	3.71	–	–	$I = 0.10$ M in Na^+ ionic medium	[37]
L4	9.85	9.01	3.83	1.35	$I = 0.10$ M in $KNO_{3(aq)}$	[15]
L5	10.07	9.09	3.20	–	$I = 0.10$ M in $KCl_{(aq)}$	[17]

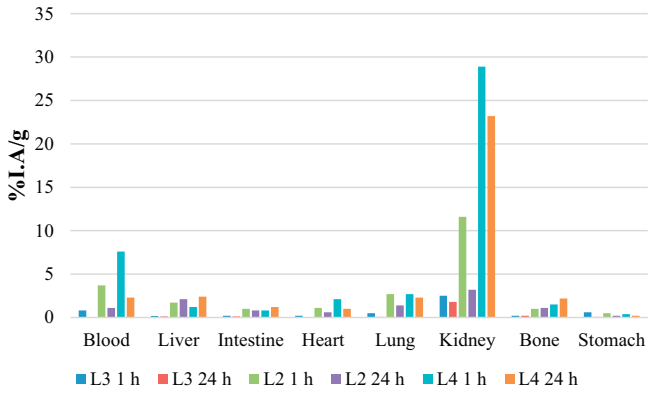

Fig. 7. Biodistribution data in the most relevant organs of ^{67}Ga-citrate after intraperitoneal injection of *L3*, *L2* or *L4* expressed as % I. A./g, 1, and 24 h post-injection in female Balb-C mice (n = 3).

biodistribution and radioactivity excretion of the radionuclide with intraperitoneal injection of 0.5 μmole of the ligand solution immediately after intravenous administration of the radiotracer was compared with the well established distribution of the radiotracer, in the same animal model.

Biodistribution profiles of ^{67}Ga in the main organs and tissues after administration of the different chelators, at 1 h and 24 h are presented in Fig. 7, while the corresponding excretion profiles are reported in Fig. 8, in comparison with those of DFP. Analysis of data clearly indicates that the co-administration of any of the ligands interferes in the tissue distribution of the radiometal, inducing a faster clearance from blood and from the main organs and from whole body. These findings are in accordance with the effects induced in the distribution and excretion of ^{67}Ga by other similar ligands, including *L1*, *L4* and *L5*, reported in previous papers [15,16]. However, a direct comparison cannot be made, since those results were obtained with different mice strains. Furthermore, analysis of the bioassays results clearly indicates modifications induced on the usual ^{67}Ga biodistribution profiles depending on the extra-functional groups. The most striking differences are related with the blood clearance, kidney uptake and retention and the rate of total excretion, that is significantly faster after co-administration of *L3* than any of the other ligands (*L2*, *L4*). In fact, all these 3-hydroxy-4-pyridinones present a similarly high chelating capacity in solution, attributed to cooperation of the terminal amino-carboxylic group. However, the *in vivo* metal uptake (sequestration) depends also on the pharmacokinetic properties and, importantly, on the interaction of the ligands (and corresponding metal-complexes) with metal-binding plasma proteins, such as transferrin and albumin, which for Al^{3+} in human plasma can exist in concentrations ~60 and 30%, respectively [49]. Indeed the small structural differences of the extra-functional groups of these three bioassayed compounds resulted in different molecular descriptors (*see* Table 7). Therefore, since out of the three compounds, *L4* presents the lowest MW, highest lipophilicity and strongest interaction with Human Serum Albumin (HSA), it is likely that *L4* and its complex have higher interaction with other proteins, with concomitantly slower blood clearance and higher kidney retention along the renal excretion.

Finally, taking *L3* as a representative example of these extra-functionalized 3,4-HP chelators, the biodistribution and excretion profiles of ^{67}Ga after administration of *L3* at 1 h and 24 h, in comparison with those of ^{67}Ga-citrate and deferiprone (DFP) is presented in Fig. 9. Comparison of the metal biodistribution profiles, induced by our *L3* ligand and by the iron-chelating drug DFP at the same experimental conditions, indicates that the co-administration of the ligand *L3* enhanced the clearance of the radiometal ^{67}Ga and the overall excretion rate of radioactivity from whole animal body more efficiently than the drug. In fact, at 1 h, 66.1% ± 4.9 of the injected activity was already eliminated, while after administration of DFP only 26.5% of I.A. was excreted. Altogether these results suggest that, in our animal model, the radiometal ion is very efficiently chelated by the 3-hydroxy4-pyridinones functionalized with an amino-carboxylic side chain, in particular by the ligand *L3*, which appears as a very promising metal sequestering agent.

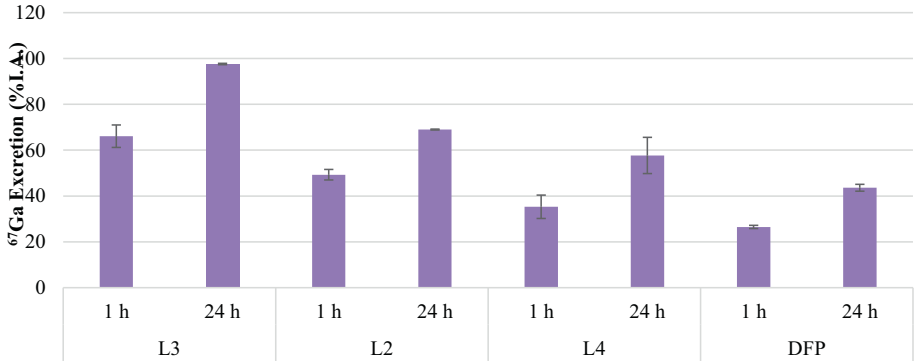

Fig. 8. Excretion of ^{67}Ga-citrate after intraperitoneal injection of *L3*, *L2*, *L4* and DFP expressed as % I. A. 1, and 24 h post-injection in female Balb-C mice (n = 3).

Table 7
Pharmacokinetic properties as predicted *in silico* by software QikProp v.2.5 [54].

Comp.	MW	Donors H bonds	Acceptors H bonds	clog*P* O/W	log*K* HSA serum binding	log BB	% Human oral absorpt. GI
DFP	139	1	3.25	0.601	−0.554	−0.296	78
L1	211	2	5.25	0.723	−0.708	−1.587 −	41
L2	283	4	7.75	−2.815	−1.151	−2.417 −	16
L3	297	4	7.75	−2.632	−1.704	−2.507	21
L4	240	4	6.25	−2.082	−0.800	−1.655	33
L5	182	3	4.25	−0.150	−0.584	−0.747	62

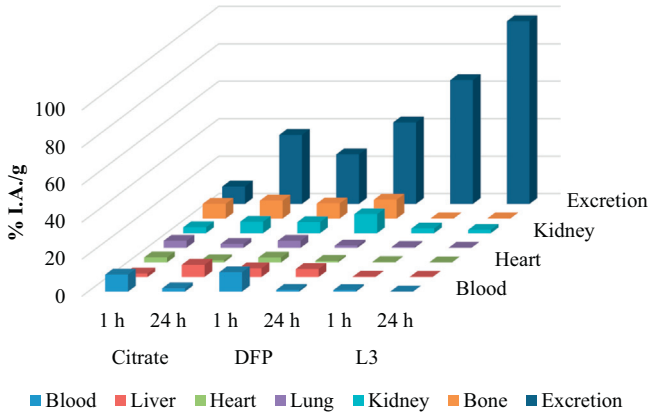

Fig. 9. Biodistribution of ^{67}Ga-citrate and ^{67}Ga-citrate after intraperitoneal injection of *L3* or DFP expressed as % I. A./g, 1, and 24 h post-injection in female Balb-C mice (n = 3).

3.9. Pharmacokinetic properties

To evaluate the drug-likeness of the 3,4-hydroxypyridinones in study, some descriptors of their pharmacokinetic profiles were calculated using QikProp program, v. 2.5 [54]. Thus, parameters such as the calculated octanol–water partition coefficient (clog*P*), the ability to cross the BBB (log BB), the capacity to be absorbed through the gastrointestinal gut, and binding with human serum albumin, have been calculated and are summarized in Table 7. Analysis of the data in this table show that all the compounds, presented appropriate lipophilicity (clog*P* < 5), molecular weights (< 500) and number of H-bond acceptors (< 10) or H-bond donors (< 5). All the compounds fulfill the criteria for the Lipinski's rule of five [55], thus indicating a good bioavailability and oral activity as potential drugs. Furthermore, the compounds *L2*, *L3*, *L4* with the best metal sequestering capacity are more hydrophilic than the others, but they present good capacity for membrane permeation as indicated by log BB values (> −3), the highest binding interaction with Human serum albumin (HSA), and moderate % Human oral absorption by the gastrointestinal (GI) track [54]. Conversely the other compounds (DFP, *L1* and *L5*) presented higher lipophilicity and % GI absorption but less interaction with HSA and lower metal sequestering capacity.

4. Conclusions

A set of extrafunctionalized 3-hydroxy-4-pyridinones (3,4-HPs) was synthesized; their acid-base properties and binding ability towards the metal cation Al^{3+} in NaCl aqueous solutions were investigated in solution and the *in vivo* sequestering capacity was studied. The new 3-hydroxy-4-pyridinones were prepared from a naturally occurring compound (*i.e.* maltol) and *N*-functionalized to introduce differentiation in terms of pharmacokinetic parameters and interaction with proteins, while keeping the bioavailability parameters. The acid-base behavior and the binding ability of these 3,4-HPs towards the Al^{3+} were studied through potentiometric and UV–Vis spectrophotometric experiments carried out at T = 298.15 K and I = 0.15 M in $NaCl_{(aq)}$. The speciation models were characterized by $Al_pL_qH_r^{(3p+r-qz)}$ species with different stoichiometry, such as simple metal-ligand (1:1 stoichiometry) and polynuclear species, depending on the ligands different charges and structures.

From data obtained it was concluded that the stability of $[AlL]^{(3-z)}$ species follows the trend:

L4 > *L2* > *L3* > *L5* > *L1*

Furthermore, for *L2*, the models proposed for its protonation as well as for *L2* complexing ability towards Al^{3+} were confirmed by ^{1}H NMR investigations, which clearly indicated that the coordination of Al^{3+} occurs *via* the hydroxo-oxo bidentate moiety of the hydroxypyridinone side of the ligand. However, based on HypNMR calculations for the complex species, it is suggested that, in some cases, the terminal side-chain carboxylate groups may also interact with Al^{3+}. The sequestering ability of the 3-hydroxy-4-pyridinones towards aluminium was investigated by the calculation of the $pL_{0.5}$ values, highlighting that the presence of carboxylic groups in the ligands enhances their affinity towards Al^{3+}, since the trend *L2* > *L4* > *L3* > *L1* > *L5* was observed. Finally, the *in vivo* metal sequestration indicates for *L2*, *L3* and *L4* a higher capacity for metal clearance than the drug DFP, thus appearing as promising aluminium chelating drugs.

Acknowledgements

The authors from the University of Messina thank MIUR (Ministero dell'Istruzione, dell'Università e della Ricerca) for financial support (co-funded PRIN project with prot. 2015MP34H3).

The authors from (IST) University of Lisbon thank the Portuguese Fundação para a Ciência e a Tecnologia (FCT) for financial support to the projects UID/QUI/00100/2013 and PEst-C/SAU/LA0001/2011-2013, and the postdoctoral fellowship (KC). Acknowledgements are also due to the Portuguese NMR (IST-UL Center) and Mass Spectrometry Networks (Node IST-CTN) for providing access to their facilities.

Appendix A. Supplementary data

Supplementary data to this article can be found online at https://doi.org/10.1016/j.jinorgbio.2018.05.017.

References

[1] S. Chaves, L. Piemontese, A. Hiremathad, M.A. Santos, Curr. Med. Chem. 25 (2018) 97–112.
[2] G. Crisponi, V.M. Nurchi, V. Bertolasi, M. Remelli, G. Faa, Coord. Chem. Rev. 256 (2012) 89–104.
[3] Z.D. Liu, R.C. Hider, Medicinal Research Reviews, 22 John Wiley & Sons, Inc., 2002, pp. 26–64.
[4] M.A. Santos, S. Chaves, Future Med. Chem. 7 (2015) 383–410.
[5] S. Gama, P. Dron, S. Chaves, E. Farkas, M.A. Santos, Dalton Trans. (2009) 6141–6150.
[6] J.B. Neilands, Annu. Rev. Biochem. 50 (1981) 715–731.
[7] G. Anderegg, F. L'Eplattenier, G. Schwarzenbach, Helv. Chim. Acta, 46 WILEY-VCH Verlag GmbH, 1963, pp. 1400–1408.
[8] B.J. Hernlem, L.M. Vane, G.D. Sayles, Inorg. Chim. Acta 244 (1996) 179–184.
[9] J.B. Porter, E.R. Huehns, Baillieres Clin. Haematol. 2 (1989) 459–474.
[10] M.A. Santos, Coord. Chem. Rev. 252 (2008) 1213–1224.
[11] M.A. Santos, M.A. Esteves, M.C.T. Vaz, M.L.S.S. Gonçalves, J. Chem. Soc. Dalton Trans. (1993) 927–932.
[12] M.A. Santos, S. Gama, L. Gano, G. Cantinho, E. Farkas, Dalton Trans. (2004) 3772–3781.
[13] M.A. Santos, S. Gama, L. Gano, E. Farkas, J. Inorg. Biochem. 99 (2005) 1845–1852.
[14] G.J. Kontoghiorghes, L.N. Sheppard, T.A. Cresswell, et al. (Ed.), E.P. Office, J. A. Kemp & Co., 14 South Square Gray's Inn, London WC1R 5EU (GB), EP 0 335 745 A1, Great Britain, 1989, pp. 1–22.
[15] M.A. Santos, M. Gil, L. Gano, S. Chaves, J. Biol. Inorg. Chem. 10 (2005) 564.
[16] M.A. Santos, M. Gil, S. Marques, L. Gano, G. Cantinho, S. Chaves, J. Inorg. Biochem. 92 (2002) 43–54.
[17] M.A. Santos, R. Grazina, A.Q. Neto, G. Cantinho, L. Gano, L. Patrıcio, J. Inorg. Biochem. 304 (2000) 303–311.
[18] J. Buffle, Complexation Reactions in Aquatic Systems: An Analytical Approach, (1988).
[19] F.J. Millero, Physical Chemistry of Natural Waters, (2001).
[20] C. Lentner, Geigy Scientific Tables, (1981).
[21] A. Gianguzza, O. Giuffrè, D. Piazzese, S. Sammartano, Coord. Chem. Rev. 256 (2012) 222–239.
[22] H.A. Flaschka, EDTA Titration, (1959).
[23] W.L.F. Armarego, D.D. Perrin, Purification of Laboratory Chemicals, (1999).
[24] M.A. Santos, M. Gil, S. Marques, L. Gano, G. Cantinho, S. Chaves, J. Inorg. Biochem. 92 (2002) 43–54.
[25] A. Braibanti, G. Ostacoli, P. Paoletti, L.D. Pettit, S. Sammartano, Pure Appl. Chem. 59 (1987) 1721.
[26] C. De Stefano, P. Princi, C. Rigano, S. Sammartano, Ann. Chim. 7 (1987) 643–675.
[27] P. Gans, A. Sabatini, A. Vacca, Talanta 43 (1996) 1739–1753.

[28] C. Frassineti, S. Ghelli, P. Gans, A. Sabatini, M.S. Moruzzi, A. Vacca, Anal. Biochem. 231 (1995) 374–382.
[29] C. De Stefano, S. Sammartano, P. Mineo, C. Rigano, A. Gianguzza, E. Pelizzetti, S. Sammartano (Eds.), Marine Chemistry - An Environmental Analytical Chemistry Approach, Kluwer Academic Publishers, Amsterdam, 1997, pp. 71–83.
[30] C. Agouridas, A. Denis, J.-M. Auger, Y. Benedetti, A. Bonnefoy, F. Bretin, J.-F. Chantot, A. Dussarat, C. Fromentin, S.G. D'Ambrières, S. Lachaud, P. Laurin, O. Le Martret, V. Loyau, N. Tessot, J. Med. Chem. 41 (1998) 4080–4100.
[31] A.W. Williamson, Justus Liebigs Ann. Chem. 77 (1851) 37–49.
[32] A.W. Williamson, Quart. J. Chem. Soc. 4 (1852) 229–239.
[33] R.L.N. Harris, Aust. J. Chem. 29 (1976) 1335–1339.
[34] L. Saghaie, M.M. Sadeghi, A. Nikazma, Res. Pharm. Sci. 1 (2006) 40–48.
[35] C.F. Baes, R.E. Mesmer, John Wiley & Sons, New York (1976).
[36] R.M. Cigala, C. De Stefano, A. Giacalone, A. Gianguzza, Chem. Speciat. Bioavailab. 23 (2011) 33–37.
[37] A.E. Martell, R.M. Smith, R.J. Motekaitis, NIST Critically Selected Stability Constants of Metal Complexes Database, 8.0 (2004).
[38] F.J. Millero, R. Woosley, Environ. Sci. Technol. 43 (2009) 1818–1823.
[39] D. Pettit, K.K. Powell, Stability Constants Database, Academic Software, (1997).
[40] P. Cardiano, R.M. Cigala, F. Crea, F. Giacobello, O. Giuffrè, A. Irto, G. Lando, S. Sammartano, Chemosphere 186 (2017) 535–545.
[41] L.O. Öhman, Department of Inorganic Chemistry, University of Umeà, Sweden, 1983.
[42] L. Alderighi, P. Gans, A. Ienco, D. Peters, A. Sabatini, A. Vacca, Coordin, Chem. Rev. 184 (1999) 311–318.
[43] S. Chaves, M. Gil, S. Marques, L. Gano, M.A. Santos, J. Inorg. Biochem. 97 (2003) 161–172.
[44] D. Aiello, P. Cardiano, R.M. Cigala, P. Gans, F. Giacobello, O. Giuffrè, A. Napoli, S. Sammartano, J. Chem. Eng. Data 62 (2017) 3981–3990.
[45] P. Cardiano, F. Giacobello, O. Giuffrè, S. Sammartano, J. Mol. Liq. 232 (2017) 45–54.
[46] F. Crea, C. De Stefano, C. Foti, D. Milea, S. Sammartano, Curr. Med. Chem. 21 (2014) 3819–3836.
[47] C. Bretti, R.M. Cigala, F. Crea, G. Lando, S. Sammartano, J. Chem. Thermodyn. 77 (2014) 98–106.
[48] D.J. Clevette, W.O. Nelson, A. Nordin, C. Orvig, S. Sjoeberg, Inorg. Chem. 28 (1989) 2079–2081.
[49] R. Ma, J.J. Reibenspies, A.E. Martell, Inorg. Chim. Acta 223 (1994) 21–29.
[50] G. Crisponi, V.M. Nurchi, M.A. Zoroddu, Thalassemia Reports, 4 (2014), p. 2046.
[51] G. Crisponi, M. Remelli, Coord. Chem. Rev. 252 (2008) 1225–1240.
[52] V.M. Nurchi, G. Crisponi, T. Pivetta, M. Donatoni, M. Remelli, J. Inorg. Biochem. 102 (2008) 684–692.
[53] E.T. Clarke, A.E. Martell, Inorg. Chim. Acta 191 (1992) 57–63.
[54] L.L.C. Schrödinger, New York, NY, (2005).
[55] C.A. Lipinski, F. Lombardo, B.W. Dominy, P.J. Feeney, Adv. Drug Deliv. Rev. 46 (2001) 3–26.